







## Article

# Linear/Nonlinear Optical Characteristics of ZnO-Doped PVA/PVP Polymeric Films for Electronic and Optical Limiting Applications

Samer H. Zyoud <sup>1,2,3,\*</sup> , Thekayat H. AlAbdulaal <sup>4</sup>, Ali Almoadi <sup>4,5</sup>, Mohammed S. Alqahtani <sup>5,6</sup> , Farid A. Harraz <sup>7,8</sup> , Mohammad S. Al-Assiri <sup>7,9</sup>, Ibrahim S. Yahia <sup>3,4,10,11</sup> , Heba Y. Zahran <sup>4,10,11</sup> , Mervat I. Mohammed <sup>11</sup> and Mohamed Sh. Abdel-wahab <sup>12</sup> 

- <sup>1</sup> Department of Mathematics and Sciences, Ajman University, Ajman P.O. Box 346, United Arab Emirates
- <sup>2</sup> Nonlinear Dynamics Research Center (NDRC), Ajman University, Ajman P.O. Box 346, United Arab Emirates
- <sup>3</sup> Center of Medical and Bio-Allied Health Sciences Research (CMBHSR), Ajman University, Ajman P.O. Box 346, United Arab Emirates
- <sup>4</sup> Laboratory of Nano-Smart Materials for Science and Technology (LNSMST), Department of Physics, Faculty of Science, King Khalid University, Abha P.O. Box 9004, Saudi Arabia
- <sup>5</sup> Department of Radiological Sciences, College of Applied Medical Sciences, King Khalid University, Abha 61421, Saudi Arabia
- <sup>6</sup> BioImaging Unit, Space Research Centre, Department of Physics and Astronomy, University of Leicester, Leicester LE1 7RH, UK
- <sup>7</sup> Promising Centre for Sensors and Electronic Devices (PCSED), Advanced Materials and Nano-Research Centre, Najran University, P.O. Box 1988, Najran 11001, Saudi Arabia
- <sup>8</sup> Nanomaterials and Nanotechnology Department, Central Metallurgical Research and Development Institute (CMRDI), P.O. Box 87, Cairo 11421, Egypt
- <sup>9</sup> Department of Physics, Faculty of Science and Arts, Najran University, P.O. Box 1988, Najran 11001, Saudi Arabia
- <sup>10</sup> Research Center for Advanced Materials Science (RCAMS), King Khalid University, P.O. Box 9004, Abha 61413, Saudi Arabia
- <sup>11</sup> Nanoscience Laboratory for Environmental and Biomedical Applications (NLEBA), Semiconductor Laboratory, Metallurgical Lab.1., Department of Physics, Faculty of Education, Ain Shams University, Cairo 11757, Egypt
- <sup>12</sup> Materials Science and Nanotechnology Department, Faculty of Postgraduate Studies for Advanced Sciences, Beni-Suef University, Beni-Suef 62511, Egypt
- \* Correspondence: s.zyoud@ajman.ac.ae



**Citation:** Zyoud, S.H.; AlAbdulaal, T.H.; Almoadi, A.; Alqahtani, M.S.; Harraz, F.A.; Al-Assiri, M.S.; Yahia, I.S.; Zahran, H.Y.; Mohammed, M.I.; Abdel-wahab, M.S. Linear/Nonlinear Optical Characteristics of ZnO-Doped PVA/PVP Polymeric Films for Electronic and Optical Limiting Applications. *Crystals* **2023**, *13*, 608. <https://doi.org/10.3390/cryst13040608>

Academic Editor: Giuseppe Prestopino

Received: 16 January 2023

Revised: 7 March 2023

Accepted: 8 March 2023

Published: 2 April 2023



**Copyright:** © 2023 by the authors. Licensee MDPI, Basel, Switzerland. This article is an open access article distributed under the terms and conditions of the Creative Commons Attribution (CC BY) license (<https://creativecommons.org/licenses/by/4.0/>).

**Abstract:** ZnO-doped Polyvinyl alcohol/polyvinyl pyrrolidone (PVA/PVP) polymeric films were prepared in this study through an easy and inexpensive solution-casting method. The scope of the study was based on the structural, dielectric, and optical parameters, as well as on the optical limiting effects of the ZnO-doped polymer blend (PB) as nanocomposite films. The X-ray diffraction (XRD) analysis indicated that the synthesized nanocomposites were semicrystalline. The calculated crystalline size of the polymeric semicrystalline peak decreased as ZnO increased or enhanced the blend polymer. Fourier's transformer infrared (FT-IR) study confirmed a substantial dispersion of ZnO nanoparticles in a polymeric PVA/PVP matrix. The optical absorption properties suggested focusing on the surface plasmonic peak (SPR). The refractive index values ranged from 1.718 for the pure PB ZnO<sub>0</sub> sample in the Hossam, Ibrahim, and Heba model to 3.036 for the PB ZnO<sub>5</sub> film from the Anani model. Nonlinear optical parameters ( $\chi^{(3)}$ , and  $n(2)$ ) were calculated and analyzed for the PB ZnO nanocomposite films under investigation. The maximum value for  $\chi^{(1)}$  was 0.550, while for  $\chi^{(3)}$ , its susceptibility value was  $155.85 \times 10^{-13}$  esu, and for the nonlinear refractive index ( $n^{(2)}$ ), it was  $20.87 \times 10^{-11}$  esu. A gradual decrease was revealed in the optical limiting sources, as a high content of ZnO was induced in the blend PVA/PVP polymer. Due to their unique properties, these materials can be used in electronic and optoelectronic devices.

**Keywords:** zinc oxide doped PVA/PVP; PVA/PVP blend polymers; nanocomposite films; XRD/FT-IR; nonlinear optical properties; optical laser limiting; nonlinear I–V curves

## 1. Introduction

It is currently known that exposure to UV radiation has a dramatic and significant impact in terms of damage to human eyes. Additionally, UV-radiation degrades the oxygen layer of atoms on materials. When chemical bonds in polymers are broken, radicals (atoms or molecules with unpaired electrons) can form, which are highly reactive and contribute to the UV-induced damage mechanism. When these radicals come into contact with nearby free bonds, they can split or degrade the polymer molecules. Oxidation and hydrolysis degradation mechanisms can also occur when UV-dissociated bonds react with available oxygen or water, typically on the polymer's surface. The various degradation mechanisms have been discussed abstractly, but in practice, they often occur together and have a synergistic effect. Absorption of high-energy UV photons can boost electrons to higher energy levels and dissociate the chemical bonds, leading to chemical and microstructural changes in the material [1]. Therefore, considerable critical attention is being paid to finding a material that protects against UV radiation.

Semiconductor materials have yielded valuable information beyond the most advanced knowledge in the technological field in recent years. These materials have essential widespread applications, including—VI semiconductor materials, such as solar cells, light-emitting devices [2], infrared-red windows [3], and photonics applications [4]. Zinc oxide (ZnO) is particularly significant among these materials due to its unique properties. With a wide bandgap energy of 3.37 eV, ZnO is a great UV absorber [5]. ZnO nanoparticles serve as inorganic fillers with high refractive indices, enormous excitation binding energy (60 meV) [6], chemical [7], and thermal stability, non-toxicity, and biocompatibility [8]. Doping with suitable materials could enhance the material's optical and electrical characteristics. Despite being primarily recognized as an antifungal and antibacterial agent [9,10], ZnO is increasingly being employed in electronic sensing [11], luminescent and laser devices [12,13], and as a transport electron layer in perovskite solar cells [14]. Researchers have used various methods to synthesize ZnO nanoparticles, including homogenous precipitation [15], spray pyrolysis [16], mechanical milling [17], etc.

Recent research has demonstrated the benefits of using inorganic nanofillers in preparing polymeric nanocomposites. For example, integrating semiconductor materials as nanofillers doped onto polymer membranes has attracted critical attention due to their potential applications in optics and electronics [18,19]. The high miscibility of these materials on polymeric membranes explains the complexity of their interaction [20], although it is important to note that adding nanofillers to the polymer matrix can alter the properties of the polymer itself [21]. Blending different polymers can yield exceptional properties compared to a single polymer, but it is essential to consider the uncertainties involved in achieving thermal stability and defining compound properties [22]. Blending polymers has been successfully applied in various fields, including rubbers, plastics, and composites [23–25]. For example, a blend of two suitable polymers, polyvinyl alcohol (PVA) and polyvinyl pyrrolidone (PVP), have properties tailored to specific applications and is biodegradable, non-toxic, easy to handle, commercially available, and water-soluble [26–29]. However, these properties depend not only on individual polymers but also on the phase morphology of the blend [30], which plays a significant role in determining the blend's overall properties. The emergence of hydrogen bonding between PVA and PVP is a notable characteristic of their mixture [31], which has opened the door for the development of PVA/PVP blends for use in wound dressings [32], articular cartilage replacement [33], and as a host for high-energy electrochemical devices [34].

Despite various techniques for synthesizing blended polymers, the solution casting method frequently performs the specific precision task of dispersing the blended polymers uniformly. Given the technique's simplicity, one or more polymers dissolved in an excellent solvent are required. Simultaneously, nanofillers in the blended polymer enhance the properties of the resulting materials. However, doping blended polymers with transition metal oxides has sparked a new research interest. Establishing a doping procedure addresses promising applications, such as optics, photonics, and electronics fields [35–38]. Previously

published studies on ZnO-doped PVA/PVP attempted to investigate the nanocomposite in various ways. Shobhna Choudhary et al. proposed the essential aspects of the solution-casting method for synthesizing nanocomposites [39].

Additionally, significant enhancements in nanocomposite properties led to advanced applications. M.T. Ramesan et al.'s studies demonstrated the impact of blending polymers on ZnO and revealed electrical, optical, structural, and morphological enhancements in nanocomposite films [40]. Elham Gharoy Ahangar et al. published a paper describing the PVA/ZnO nanocomposite, showing these materials' preparation process and characterization [41]. Upon careful analysis of the researched literature, it becomes evident that blended polymers doped with ZnO are widely prevalent. The present study focuses on synthesizing nanocomposite films by incorporating ZnO into PVA/PVP blends. The solution casting method is utilized to create these nanocomposites. The process involves the addition of 80 wt% PVA and 20 wt% PVP, followed by heating the mixture on a hot plate at 60 °C for roughly eight hours.

The PVA/PVP blended polymer was uniformly dispersed with varying ZnO weight percentages (wt%). The mixed polymers were then dried in an oven for a week to create transparent nanocomposite films. The higher content of ZnO-doped blended polymer slightly decreased the transparency of the films. Extensive investigations were conducted to evaluate the nanofiller's contribution to the blended polymer. The exceptional properties indicate that the suggested PVA/PVP doped with ZnO nanocomposite has immense potential for suitable applications in optoelectronics, cut-off lasers, and electronics.

Further data collection from XRD and FT-IR in our work determined the structural and morphological effects on the studied nanocomposite films. In addition, optical properties and their related parameters were investigated, and dielectric and electrical studies were examined in detail. The current–voltage ( $I$ – $V$ ) relationship was used to demonstrate the varistor applications of the studied nanocomposite films.

## 2. Materials and Synthesizing Methods

### 2.1. Materials

The Loba Chemie products, namely polyvinyl alcohol (PVA) with a degree of hydrolysis of 99% and a molecular weight of 27,000 g/mol, as well as polyvinyl pyrrolidone (PVP) with a molecular weight of 58,000 g/mol, were utilized in the preparation of zinc oxide (ZnO) nanoparticles (NPs) via sol-gel/auto-combustion methods. The metal salt used was 5 g of  $\text{Zn}(\text{NO}_3)_2 \cdot 6\text{H}_2\text{O}$ , while 5 g of citric acid was used as fuel. The solution underwent drying at 80 °C, forming a dry gel that was then heated at 550 °C for 3 h to complete the formation of ZnO nanoparticles. Our team had previously reported this technique in a published paper. It is important to note that all synthesis procedures utilized distilled water (DI).

### 2.2. Characterisation Techniques

The XRD patterns of PVA/PVP- $x$  ZnO NP films were measured in reflection mode at a scan rate of 0.05 degrees/s, using  $\text{CuK}\alpha$  radiation and  $\lambda = 1.5406 \text{ \AA}$ , with a Shimadzu LabX-XRD-6000 model. The XRD was used to investigate the crystallinity of the as-prepared nanocomposite films. The XRD tube was operated at a selected voltage of 30 kV and a current of 30 mA in the  $2\theta$  range of 5–70 degrees.

The chemical structure of the nanocomposite films was analyzed using an FT-IR spectrometer. The transmission spectra were plotted as a function of wave number, ranging from 400 to 4000  $\text{cm}^{-1}$ , using a Thermo Nicolet 6700 instrument.

To assess the linear optical properties ( $T(\lambda)$  and  $\text{Abs}(\lambda)$ ) in the wavelength range of 190 to 2500 nm at room temperature, a JASCO V-570 double-beam spectrophotometer was used. The absorbance and transmittance errors were both  $\pm 1\%$ .

The optical limiting effect on the nanocomposite films was measured using two laser source powers. The first laser, a green diode laser, had a wavelength of 532 nm, while the second laser, a He–Ne laser, had a wavelength of 632.8 nm. The sample was placed

at a distance of 0.1 m from the convex lens, and the lens and films were aligned with the incoming laser beam in front of the detector. Input power was measured without the sample, and the output power was measured through the samples using a sensitive laser power meter.

An automated LCR meter (FLUKE—PM6306 Model) was used to measure the AC electrical conductivity and dielectric properties of the synthesized ZnO-doped PVA/PVP polymeric films in the frequency range 100 Hz–1 MHz at room temperature. Before measurement, two copper plates were placed between the samples as an ohmic contact, and a brass electrode holder was used. The values of capacitance (C), resistance (R), and loss tangent ( $\tan\delta$ ) of the ZnO NP-doped PVA/PVP films at each excitation frequency were recorded.

Finally, the I–V characteristic curve of the as-prepared ZnO NP-doped PVA/PVP films was plotted at room temperature using a DC power supply, voltmeter, and digital Keithly electrometer 616.

### 2.3. Experimental Procedure

The polymeric nanocomposite films (doped with ZnO NPs) were prepared using the standard solution casting process. Firstly, the host matrix, consisting of PVA/PVP with a composition of 80 wt% PVA and 20 wt% PVP, was dissolved in 1 L of DI water. The mixture was continuously stirred using a magnetic stirrer on a hot plate at 80 °C for approximately eight hours to obtain a homogeneous, transparent solution.

To prepare the polymeric nanocomposite films of PVA/PVP-(xZnO NPs in g), the required weight fraction (wt%) of ZnO NPs was added to the polymeric blend solutions. The weight fractions of ZnO NPs used were  $x = 0, 0.05, 0.25, 0.5, 2.5$ , and  $5.5$  wt%. The resulting polymeric films were labeled Pure PB ZnO<sub>0</sub>, PB ZnO<sub>1</sub>, PB ZnO<sub>2</sub>, PB ZnO<sub>3</sub>, PB ZnO<sub>4</sub>, and PB ZnO<sub>5</sub>. The ZnO NPs were uniformly dispersed using ultrasonic mixing.

The homogenous mixtures were poured into perfectly flat Petri plates and left to dry at room temperature for one week to form high-quality films. Finally, the films were removed from the Petri dish and cut into the required size for further investigation, with a mean area of approximately  $2 \times 2$  cm<sup>2</sup>.

## 3. Result and Discussion

### 3.1. XRD Measurements and Analysis of ZnO-Doped PVA/PVP Nanocomposite Films

Figure 1 illustrates the XRD analysis of a pure PVA/PVP polymer containing various weight concentrations of ZnO nanocomposites at room temperature. The graph was first used to determine the peaks' intensity, deterioration, and sharpness, followed by the dopant (ZnO) dispersion on the PVA/PVP matrix. Previous findings from the XRD analysis confirmed the complex adsorption of the nanoparticles on the blend polymer. Another contributing factor to the broadening was the increase in the amorphousness of the blend polymer [42]. The peak at  $2\theta = 19.13^\circ$  indicated the semicrystalline nature of the pure PVA/PVP film, consistent with earlier studies [43]. This nature of PVA/PVP supported the presented interaction through hydrogen bonding.

With regard to ZnO, the PB ZnO<sub>5</sub> peak had the lowest intensity with the most broadening. Table 1 provides a detailed analysis of the peak position ( $2\theta$ ) and full width at half maximum ( $\beta$ ) for the blend polymers, determined through Gaussian fitting of all XRD parameters [44,45]. The peak inside the table represents the semicrystalline peak of the blend polymer, not ZnO. At the maximum doping level of ZnO (5.5 wt%), no peaks within the XRD patterns represented the ZnO phase. Any small peaks in the XRD patterns were due to the background, not the ZnO phase. Finally, the crystalline size of the nanocomposite films was calculated using the Debye-Scherrer formula [46]:

$$D = \frac{k\lambda}{\beta \cos \theta}, \quad (1)$$

where  $k$  is Scherrer's constant,  $k = 0.9$ ,  $\lambda = 0.15406$  nm, and  $\theta$  is Bragg's diffraction angle. The crystalline size tended to lower values with the introduction of ZnO NPs, which confirmed the ZnO structure films in the PVA/PVP blend polymer. In addition, the d-spacing is accounted for by Bragg's equation [47]:

$$d = \frac{\lambda}{2 \sin \theta'} \quad (2)$$

Table 1 presents the d-spacing values of all PVA/PVP-(xZnO) nanocomposite samples. The experimental values indicate an irregular interaction between the blend polymer and ZnO, as there was no significant change in d-spacing upon adding the nanofiller. However, the dislocation density is another important parameter that characterizes the defects in the nanocomposite films. The dislocation density ( $\delta$ ) was evaluated using Williamson and Smallman's formula, which is expressed by the following equation [48]:

$$\delta = \frac{1}{D^2}, \quad (3)$$

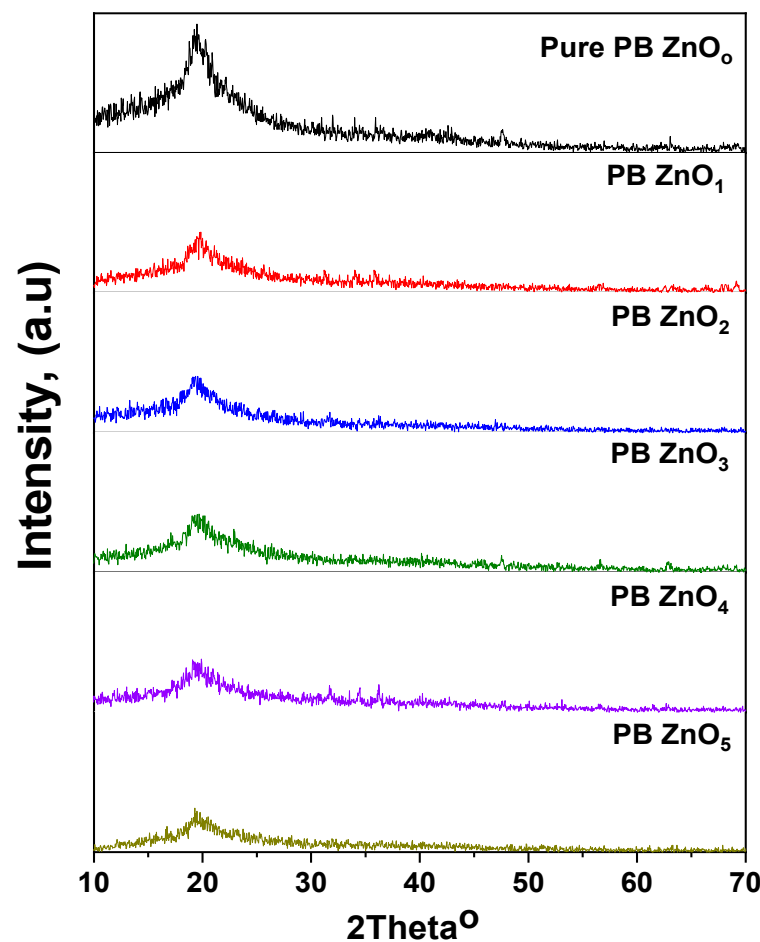


Figure 1. XRD spectra of PVA/PVP blend and ZnO polymeric nanocomposite films.



**Table 1.** The calculated values of crystalline size ( $D$ ),  $d$ -spacing, dislocation density ( $\delta$ ), and strain length ( $\epsilon$ ) of the PVA/PVP doped in ZnO nanocomposite films.

Samples	Peaks Position, (2 Theta)	FWHM, ( $\beta$ in Rad)	Crystalline Size, ( $D = \text{nm}$ )	$d$ -spacing, (Angstrom)	$\delta \times 10^{-3}, (\text{nm}^{-2})$	$\epsilon \times 10^{-3}$
Pure PB ZnO <sub>0</sub>	19.6°	0.037854	3.7	4.527	9.32	72.38
PB ZnO <sub>1</sub>	19.79°	0.040994	3.43	4.484	10.10	84.84
PB ZnO <sub>2</sub>	19.36°	0.0341911	4.11	4.583	8.426	59.09
PB ZnO <sub>3</sub>	19.77°	0.0542522	2.59	4.489	13.3	148.6
PB ZnO <sub>4</sub>	19.76°	0.06123	2.29	4.491	15.080	189.3
PB ZnO <sub>5</sub>	19.89°	0.0525077	3.23	4.462	11.258	110.8

The peaks' broadening was attributed to the micro-stress, owing to the reordering of the atoms offset on the crystalline domain from the reference lattice point and lattice faults [49]. However, microstrain relatively changes with the  $d$ -spacing of the materials. Stokes–Wilson equation deduces the average strain of the nanocomposite films [50]:

$$\epsilon = \beta/4 \tan \theta, \quad (4)$$

Table 1 summarizes the values of microstrain and dislocation density. As the concentration of ZnO increases, there is a slight increase in both the microstrain and dislocation density. One possible explanation for these results is the bond interaction between ZnO and the blend polymer. Several reports in the literature have demonstrated agreement with the XRD results obtained in this study [51,52].

### 3.2. FT-IR Analysis of ZnO-Doped PVA/PVP Nanocomposite Films

Examining the PVA/PVP-xZnO nanocomposite films in their as-prepared state involves a crucial aspect of analysis, the FT-IR investigation. The significance of FT-IR analysis lies in its ability to identify the chemical constituents of the films at different stages. Figure 2 depicts the FT-IR of the PVA/PVP doped with ZnO nanofiller. The absorption band at 3287 cm<sup>-1</sup>, which is extreme and wide, is attributed to the O-H stretching vibration of a hydroxyl group in pure PB ZnO<sub>0</sub> [53]. Another absorption band at 2938 cm<sup>-1</sup> disrupts the stretching C-H symmetric vibration [54], while the peak at 2916 cm<sup>-1</sup> is associated with pure PB ZnO<sub>0</sub> [54]. Additionally, stretching is observed at 1733 cm<sup>-1</sup> and 1657 cm<sup>-1</sup>, representing a C=O stretching and C=C stretching [55,56]. A thorough analysis of the fingerprint region reveals additional peaks centered at 1424, 1370, 1323, 1242, 1088, 918, and 844 cm<sup>-1</sup>, attributed to C-C stretch [57], CH<sub>2</sub> bending [58], CH+OH [58], -CH<sub>2</sub> wagging [58], O-H bending [58], C-H bending [59], and -CH stretching vibrations [60]. However, increasing the doping level of ZnO NPs on the PVA/PVP nanocomposite films shows little or no change in the FT-IR peaks obtained. Nevertheless, the O-H peaks' significant reduction and disappearance are observed for the PB ZnO<sub>3</sub> and PB ZnO<sub>4</sub>. These FT-IR findings can be attributed to the formation of secondary bond forces between the PVA/PVP blend polymer and the ZnO NPs. The FT-IR peaks of the ZnO doped blend polymer exhibit a slight decline compared to the host matrix, emphasizing the success of the ZnO dispersion in the PVA/PVP blend polymer. These FT-IR results for the PB ZnO polymers agree with the structural properties of Ce<sup>3+</sup> ions doped PVA/PVP composites, as reported by F. Ali et al. [53,60]. H.E. Ali et al. have also investigated the microstructural, linear, and nonlinear optical characteristics of PVP/PVA blend polymer doping with Bi-as a filler for optoelectronic applications [60].

### 3.3. UV-Vis Spectroscopy of ZnO-Doped PVA/PVP Nanocomposite Films

Figure 3a presents the UV–Vis absorption spectra of a blend polymer doped with various wt% of ZnO nanofiller in the 190 to 2500 nm wavelength range. The spectra

show a regular increase in wavelength, followed by a significant decline in absorbance values of the nanocomposite. Adding ZnO NPs to the PVA/PVP blend polymer showed a notable increase in absorbance values, indicating a strong interaction between the nanofiller and the host polymeric matrix. The UV (A-B) region exhibits an intense absorption peak at 337 nm, notably absorbing in the UV region due to the broad bandgap effect on the absorption plot contributed by ZnO [61]. It is worth noting that the lowest wavelength range showed the most sustained absorption values, particularly for PB ZnO<sub>3</sub>, PB ZnO<sub>4</sub>, and PB ZnO<sub>5</sub> polymeric films. For higher concentrations of ZnO nanofillers in blended polymeric films, the absorbance values remain constant at abs = 5 for shorter wavelengths, as the samples with high ZnO nanofillers reached the maximum absorbance values of the spectrophotometer.

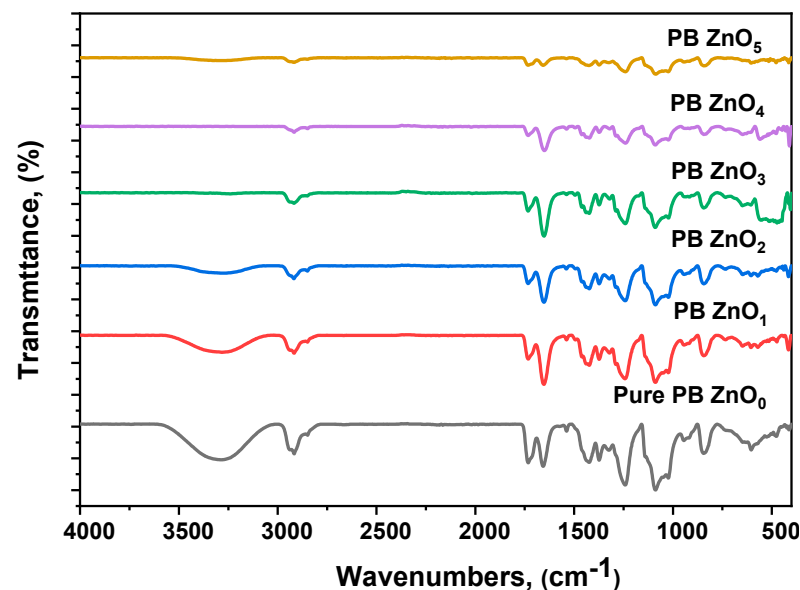


**Figure 2.** FT-IR transmittance spectra of (PVA-PVP) blend and ZnO polymeric nanocomposite films.

Consequently, the calculated optical parameters for the studied materials will be repeated as a constant value in this range. The absence of any absorption peak in the UV region raised some doubts about forming nanocomposite films. Still, a detailed review has provided valuable information on the ability of nanocomposite films in UV shielding [62,63]. Additionally, it has offered adequate evidence of the surface plasmonic resonance (SPR) feature of ZnO nanocomposite films, which is relevant for various applications, such as optoelectronics and biomedical [63]. This has been the focus of previous research in this field [64].

Figure 3b displays the transmission spectra of the PB ZnO nanocomposite films that were prepared. The transparent films were observed to have high transmission values in the visible region and low transmission values in the UV region for the pure PB ZnO<sub>0</sub> sample. The transmittance curves of the synthesized PB ZnO nanocomposites showed multi-optical oscillations in the infrared region. The addition of ZnO to the blend polymer caused a significant reduction in the transmission values compared to the pure sample, resulting in a shoulder ring-like decrease in transmission values. This decrease in transmission values was due to the influence of ZnO on the host PVA/PVP matrix, which led to surface smoothness of the films, resulting in high reflectivity and increased absorbance values [65]. Another probable reason was the scattering of the ZnO nanoparticles, which reduced the intensity of the spectral range. The PB ZnO<sub>3</sub>, PB ZnO<sub>4</sub>, and PB ZnO<sub>5</sub> samples showed a CUT-OFF or blocking of the transmission light in the wavelength range of 190 to 371 nm, indicating an extensive electronic transition in the bandgap, which was correlated with the high absorption region.

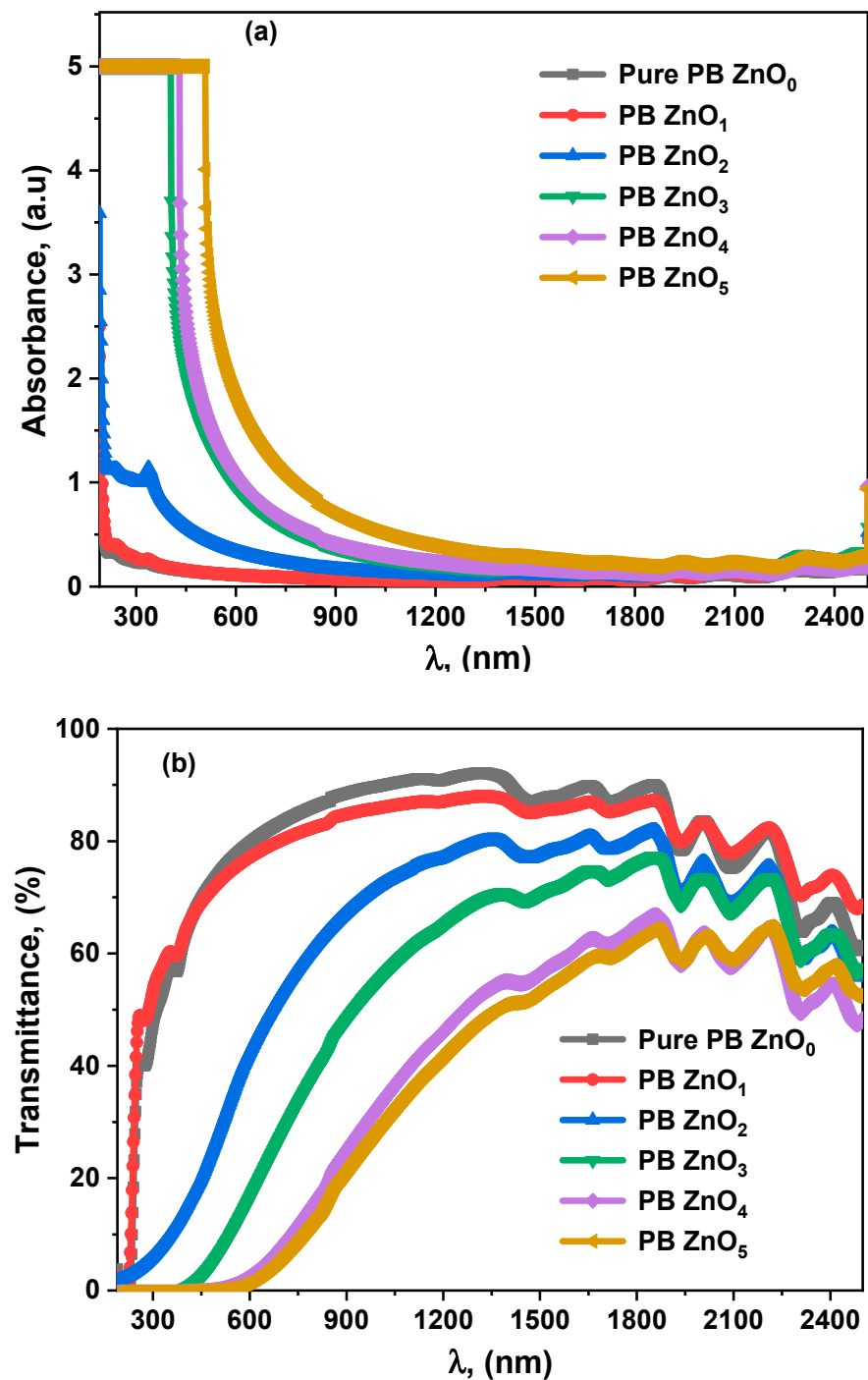


**Figure 3.** (a,b): Optical UV-Vis-NIR (a) Absorbance and (b) Transmittance curves of (PVA-PVP) blend and ZnO polymeric nanocomposite films.

Furthermore, the demonstration of these results implies the necessity to verify the efficacy of the proposed PB ZnO nanocomposite films in providing UV-protection [62]. Figure 4 illustrates ZnO's absorption coefficient ( $\alpha$ ), which was measured for varying concentrations of doped PVA/PVP polymeric films. The thickness and absorbance of the ZnO-doped PVA/PVP composite film were used to calculate the model suggested by Beer's law [66].

$$\alpha = \frac{2.304 A(\lambda)}{t}, \quad (5)$$



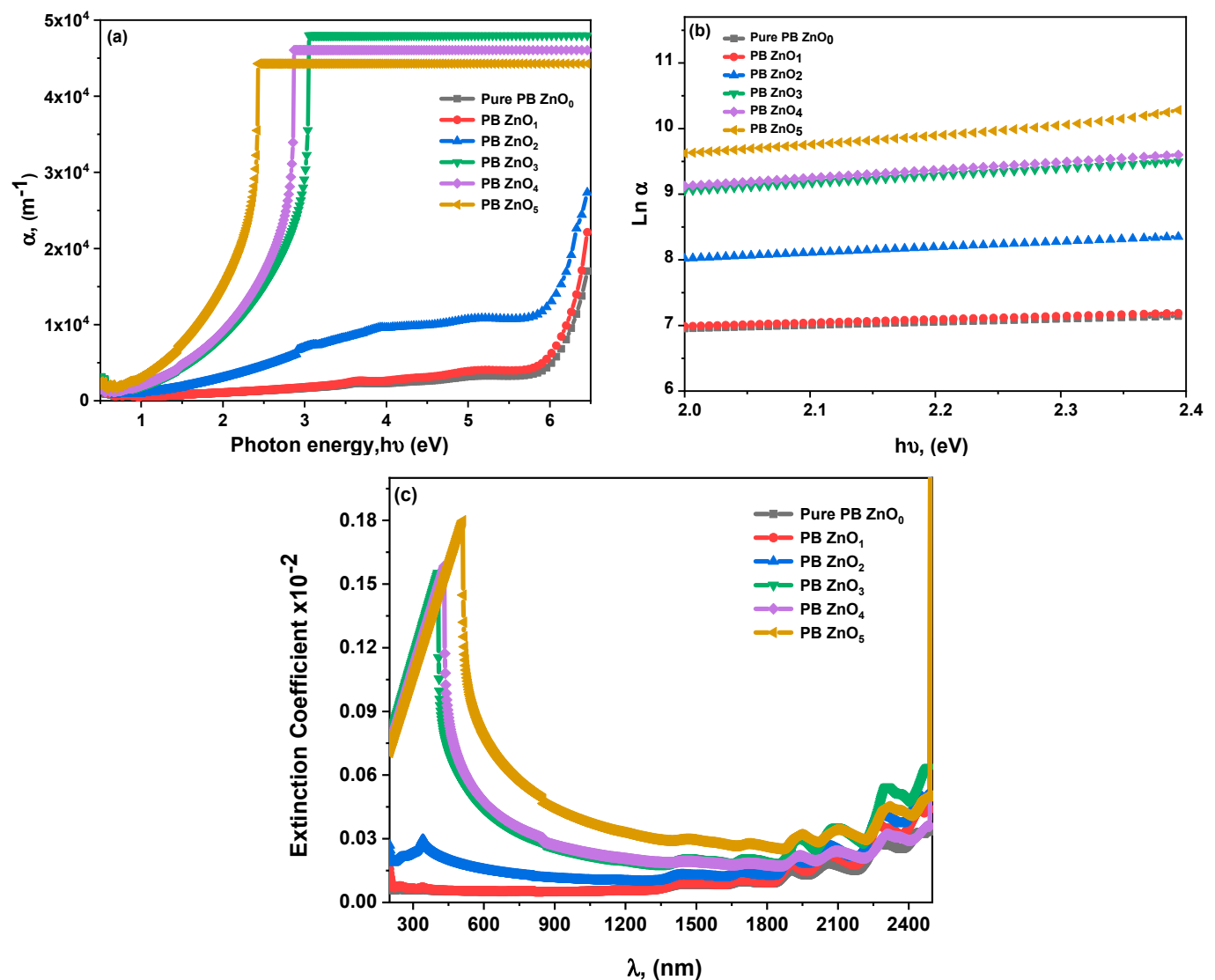


**Figure 4.** (a–c): (a) Optical absorption coefficient, (b)  $\ln \alpha$  versus  $h\nu$ , and (c) Variation of extinction coefficient as a function of wavelength for the PVA/PVP blend and ZnO polymeric nanocomposite films.

The energy bandgap of the absorption edge for the as-prepared nanocomposites can be optically determined by extrapolating  $\alpha$ , where  $t$  represents the film thickness, as shown in Table 2. Figure 4 indicates that the steepness of the  $\alpha$  curve increases with the ZnO wt% in the nanocomposites, increasing doping content and absorption coefficient. The absorption edge also gradually increases from Pure PB  $\text{ZnO}_0$  to PB  $\text{ZnO}_5$ , with extracted values of 5.95 eV and 2.01 eV, respectively. These observations demonstrate the significant impact of doping on the structure of the PVA/PVP matrix and confirm the presence of optical energy bandgaps, which contribute to the remarkable growth of semiconductors in thin films [67,68]. The extinction coefficient ( $k$ ) is a crucial optical parameter that characterizes light wave absorption in a medium, and it can be calculated using the following equation [69]:

$$k = \frac{\alpha \lambda}{4\pi}, \quad (6)$$

Figure 4c displays the extinction coefficient of the ZnO NPs-doped PVA/PVP polymeric blend films. The optical results indicated a little shift from the UV region for the  $k$  values. There was a radical increase in the  $k$  values as the high content of ZnO NPs developed in the host PVA/PVP. Moreover, the absorption peak of ZnO was addressed, but it decreased in the high wavelength region. The light scattering process was encountered

by this increase in  $k$  values from filled ZnO in the PVA/PVP polymer matrix. Tauc's power law calculates the optical absorption spectra with a relative bandgap consistent with the literature, as described in the given relation [70]:

$$(\alpha h\nu)^{\frac{1}{n}} = C (h\nu - E_g) \quad (7)$$

**Table 2.** Optical indirect/direct Bandgap of ZnO NPs-doped PVA/PVP polymeric nanocomposites.

Samples	$E_{g(ind)}$ , (eV)	$E_{g(d)}$ , (eV)	$E_{gap}^{ASF}$ , (eV)	Absorption Edge, (eV)
Pure PB ZnO <sub>0</sub>	5.69	6.06	5.09	5.95
PB ZnO <sub>1</sub>	5.45	6.002	5.04	5.87
PB ZnO <sub>2</sub>	5.16	5.92	4.7	5.7
PB ZnO <sub>3</sub>	2.56	2.96	2.53	2.6
PB ZnO <sub>4</sub>	2.11	2.76	2.31	2.39
PB ZnO <sub>5</sub>	1.82	2.37	1.89	2.01

The preceding study defined the symbols used in Equation 7. In Figure 5a,b, the optical energy bandgap was plotted for PVA/PVP blend films containing various concentrations of ZnO nanoparticles (NPs). Table 2 presents the values calculated for the direct and indirect energy bandgaps. The results indicate that the polymeric composite films' direct and indirect optical bandgap values decreased as the ZnO content increased. This decrease in the optical bandgaps is attributed to the effect of the ZnO nanofiller on the host PVA/PVP matrix, particularly at high-loaded content. Specifically, the direct energy bandgap ( $E_{g(d)}$ ) decreased from 5.69 eV to 1.82 eV for the PB ZnO nanocomposite films. However, there was no significant difference for the indirect energy bandgap ( $E_{g(ind)}$ ), which decreased slightly from 6.06 eV to 2.37 eV.

The provided data indicates the presence of a defect in the host matrix of a blend, resulting in a significant number of localized states within the bandgap [71]. Additionally, it has been observed that charge transfer complexes form within the blend matrix [72]. Lastly, it is speculated that the reduction in bandgap is due to the creation of new band levels, allowing for electron transitions from the valence band to the conduction band. This ultimately increases conductivity in the nanocomposite films under study [72]. Meanwhile, the absorption spectrum fitting (ASF) method, which employs Tauc's power law, was utilized to calculate the bandgap using the following equation [73]:

$$A(\lambda) = D\lambda \left( \frac{1}{\lambda} - \frac{1}{\lambda_g} \right), \quad (8)$$

whereas  $D = B \left( hc \right)^{m-1} \frac{d}{2.303}$ , where the complete calculation of the bandgap must pass through the equation of  $\lambda_g$ , since  $E_{gap}^{ASF} = 1240/\lambda_g$ . The variation of  $A^{1/2}/\lambda$  against  $1/\lambda$  is listed and configured in Figure 6 and Table 2, the closely relevant between the ASF and Tauc's methods. For instance, the more filled content of ZnO doped in PVA/PVP, the lowest energy bandgap was obtained. The excellent match proves the applicability of these methods to nanocomposite films.

### 3.3.1. Calculation of Refractive Index from the Energy Bandgap

The refractive index ( $n$ ) is a critical component of the optical constants, and its correlation with the energy bandgap is essential for defining the optical and electronic characteristics of semiconductors. This study focuses on optoelectronic materials and their refractive index's exponential decrease with energy bandgap. Materials with high refractive indices and large bandgap energies exhibit superior performance for optical filter and sensor applications. To understand this relationship, numerous empirical and semiempirical

equations have been proposed. Studies suggest two methods of describing the association between refractive index and energy bandgap: one directly correlates refractive index to energy bandgap. At the same time, the other uses electronegativity to calculate the bandgap and then reconstructs the refractive index. This study examines seven theoretical models Moss (Equation (9)) [74], Ravindra (Equation (10)) [75], Hervé and Vandamme (Equation (11)) [76], Reddy (Equation (12)) [77], Anani (Equation (13)) [78], Kumar and Singh (Equation (14)) [79] and Hosam, Ibrahim, and Heba (Equation (14)) [80], to investigate this relationship further and verify the computed values' validity. All equations are presented in the following:

$$n_M^4 = K/E_g, \text{ where } K = 95 \text{ eV}, \quad (9)$$

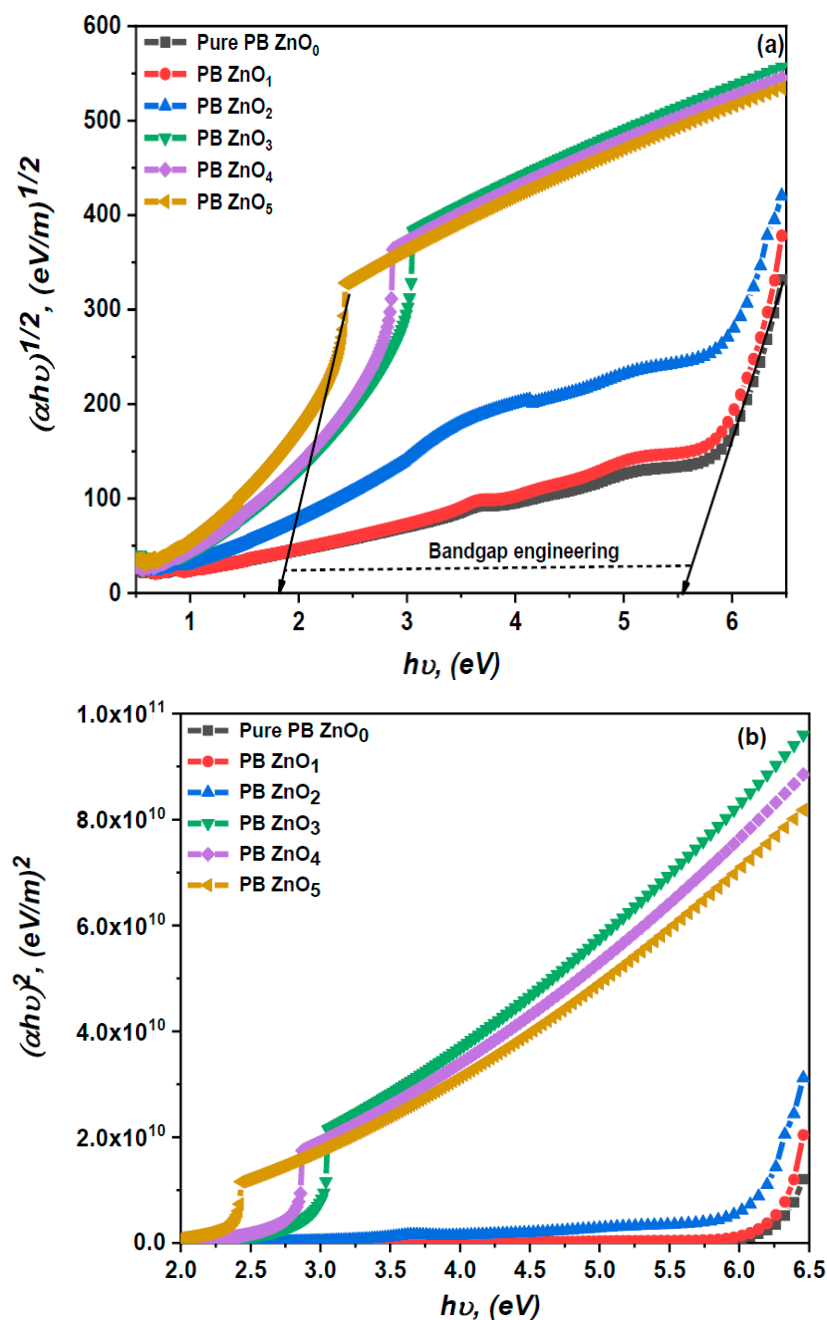


Figure 5. (a,b): Plots of (a)  $(\alpha h\nu)^{1/2}$  and (b)  $(\alpha h\nu)^2$  versus photons energy ( $h\nu$ ) for the PVA/PVP blend and ZnO polymeric nanocomposite films.

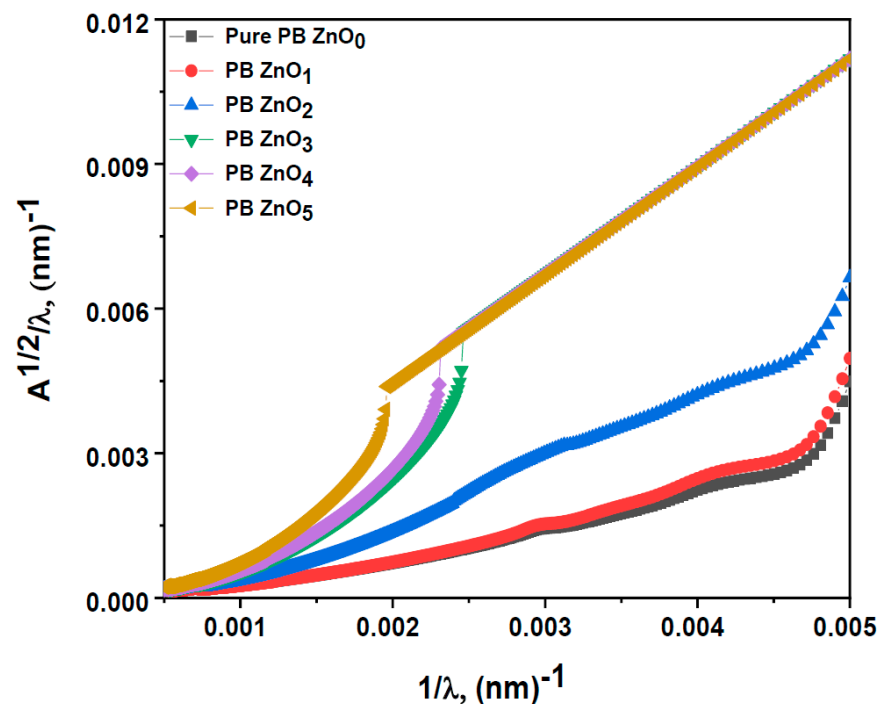


Figure 6.  $A^{1/2}/\lambda$  versus  $1/\lambda$  for PVA/PVP blend and ZnO polymeric nanocomposite films.

$$n_R^4 = K/E_g, \text{ where } K \text{ is equal to } 108 \text{ eV}, \quad (10)$$

$$n_{H,V} = \sqrt{1 + \left(\frac{13.6}{E_g + 3.4}\right)^2}, \quad (11)$$

$$n_R = \ln\left(\frac{36.3}{E_g}\right), \quad (12)$$

$$n = 3.4 - 0.2E_g, \quad (13)$$

$$n = k E_{g(\text{dir,ind})}^A, \text{ Herein } C = -0.32234 \text{ and } K = 3.3668, \quad (14)$$

$$n = \sqrt{\frac{A}{E_g^{0.5}}} - B, \text{ Herein } A = 3.442, \text{ whereas } B = \sqrt{3.44}. \quad (15)$$

Table 3a,b presents the estimated values for the refractive index obtained from the direct and indirect energy bandgap highlighting models. The mean values were computed using the equation values. Standard patterns for the seven refractive index equations from the direct and indirect energy bandgap were shown in Figure 7a,b for the ZnO-doped PVA/PVP nanocomposite films. The refractive index values obtained experimentally displayed interesting variable patterns. Specifically, the Anani model yielded the highest refractive index values for the ZnO-doped PVA/PVP nanocomposite films compared to other models. These findings offer valuable insights into the superior optical applications of the studied polymeric films.

Additionally, the refractive index values experienced significant shifts upon adding ZnO. The refractive index values ranged from 1.718 for Pure PB ZnO<sub>0</sub> in the Hossam models to 3.036 for PB ZnO<sub>5</sub> in the Anani model. The progression in the refractive index was accompanied by a substantial reduction in the bandgap, which effectively positioned the as-prepared nanocomposite materials as excellent candidates in optoelectronics [81].

**Table 3.** Calculated refractive index from Moss, Ravindra, Hervé, Reddy, Anani, Kumar- Singh, and Hossam relations and the average refractive index value for the investigated polymeric films with various adding nanofiller.

<b>(a) Indirect Band Transition.</b>								
Samples	Refractive Index Values (n): from the Indirect Bandgaps							
	Moss	Ravindra	Hervé and Vandamme	Reddy	Anani	Kumar and Singh	Hossam, Ibrahim, and Heba	Average
Pure PB ZnO <sub>0</sub>	2.021	2.087	1.799	1.853	2.262	1.922	1.762	1.958
PBZnO <sub>1</sub>	2.043	2.109	1.833	1.896	2.31	1.949	1.792	1.990
PBZnO <sub>2</sub>	2.071	2.138	1.877	1.950	2.368	1.983	1.831	2.031
PBZnO <sub>3</sub>	2.468	2.548	2.491	2.651	2.888	2.486	2.353	2.555
PBZnO <sub>4</sub>	2.590	2.674	2.663	2.845	2.978	2.646	2.508	2.700
PBZnO <sub>5</sub>	2.687	2.775	2.790	2.992	3.036	2.775	2.630	2.812
<b>(b) Direct band transition.</b>								
Pure PB ZnO <sub>0</sub>	1.989	2.054	1.751	1.790	2.188	1.883	1.718	1.910
PBZnO <sub>1</sub>	1.994	2.059	1.758	1.799	2.199	1.889	1.724	1.918
PBZnO <sub>2</sub>	2.001	2.066	1.768	1.813	2.216	1.897	1.734	1.928
PBZnO <sub>3</sub>	2.380	2.457	2.360	2.506	2.808	2.373	2.241	2.446
PBZnO <sub>4</sub>	2.422	2.501	2.423	2.5762	2.848	2.427	2.295	2.499
PBZnO <sub>5</sub>	2.516	2.598	2.560	2.728	2.926	2.549	2.414	2.613

### 3.3.2. Nonlinear Optical Parameters

A greater focus is on the nonlinearity of the nanocomposite films to examine the effectiveness of the external laser power on the films. The influence of the significant intensity source on films suggests a new term called nonlinearity. Furthermore, the developed product is associated with incident polarization and electrical field interaction. Hence, the high polarization intensity is the electric field's nonlinear function. The nonlinear polarization is conducted from the summarized relation [82]:

$$P_{NL} = \chi^{(1)}E + \chi^{(2)}E^2 + \chi^{(3)}E^3 + \dots + \chi^{(n)}E^n \quad (16)$$

where  $\chi^{(1)}$  is first-order linear optical susceptibility and  $\chi^{(2)}$  and  $\chi^{(3)}$  symbols are the second and third nonlinear optical susceptibilities. The nonlinear refractive index  $n^{(2)}$  is evaluated from the following equation [83]:

$$n(\lambda) = n^{(0)}(\lambda) + n^{(2)}(E^2), \quad (17)$$

where  $n^{(0)}$  corresponds to the linear refractive index and  $n^{(2)}$  represents the nonlinear refractive index. Various empirical relations are applied to compute those nonlinear optical parameters, as in the following equations [84,85]:

$$\chi^{(1)} = \frac{n_{AV}^2 - 1}{4\pi} \quad (18)$$

$$\chi^{(3)} = A (\chi^{(1)})^4, \text{ herein } A \text{ is constant, and } 1.7 \times 10^{-10} \text{ esu.} \quad (19)$$

$$n^{(2)} = \frac{12\pi\chi^{(3)}}{n_{AV}} \quad (20)$$

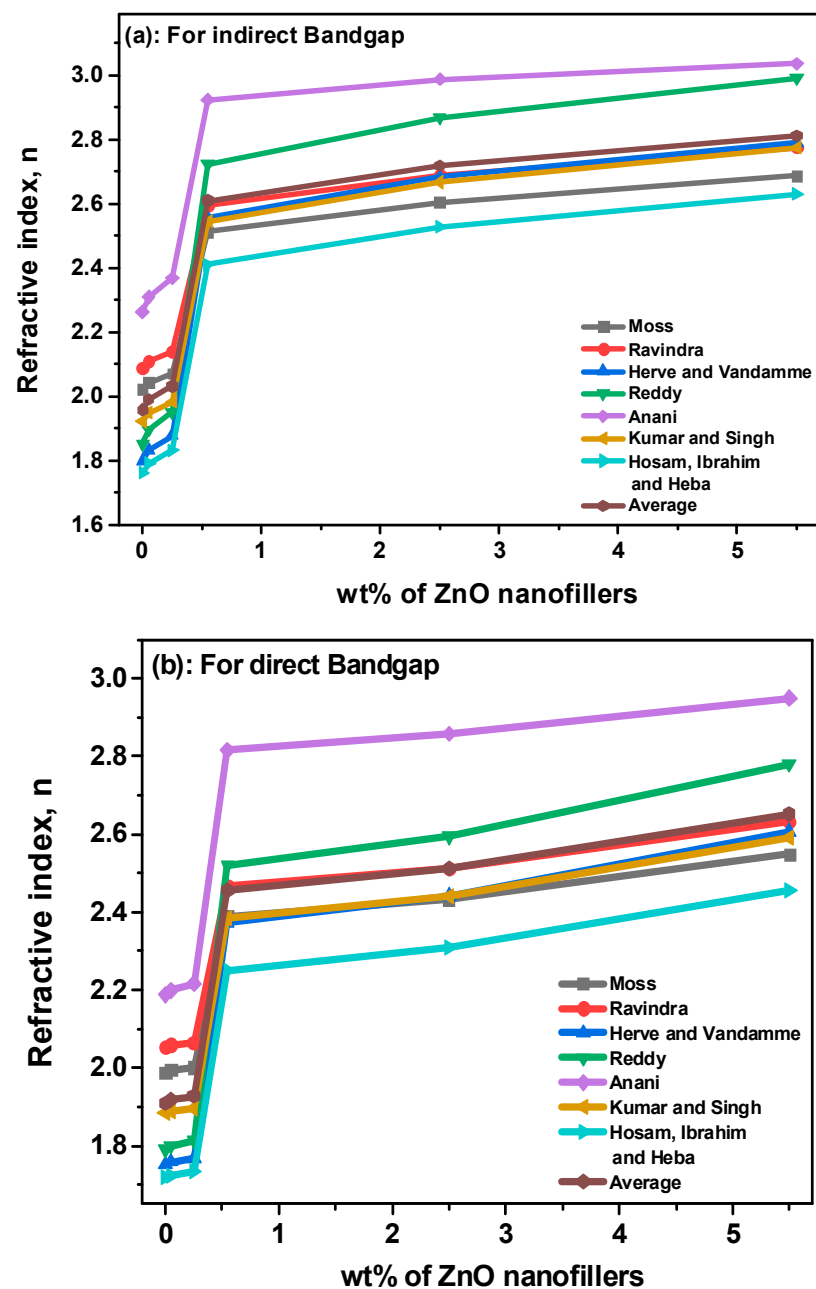


**Figure 7.** (a,b): The refractive index of different models from the indirect and direct energy bandgap is the ZnO doped in PVA/PVP polymeric nanocomposite films.

Table 4a,b demonstrates the values of the  $\chi^{(1)}$ ,  $\chi^{(3)}$ ,  $\chi^{(3)}$  as a function of the direct and indirect bandgaps for the ZnO NPs-doped PVA/PVP blend polymeric films. The integrated values of the nonlinear susceptibilities and nonlinear refractive index firmly establish a similar attitude. Further analysis suggests that the supreme values of  $\chi^{(1)}$  susceptibilities are  $155.85 \times 10^{-13}$  esu. The utmost nonlinear refractive index value is  $20.87 \times 10^{-11}$  esu for the as-proposed ZnO-doped PVA/PVP polymeric films. The calculated parameters depend on the dispersed ZnO in the host matrix. The contribution of a high concentration of ZnO-doped PVA/PVP blend polymer raises the values of the nonlinear optical parameters. These results consider these synthesized ZnO-doped PVA/PVP nanocomposite films to promote nonlinear optical applications [86]. The dielectric values of solid materials provide additional evidence offered in electronic devices. The breakthrough of such pa-



rameters as static and high-frequency dielectric constants is explored by the subsequent calculations [87]:

$$\varepsilon_{\infty} = n^2, \quad (21)$$

$$\varepsilon_0 = -33.26876 + 78.61805E_g - 45.70795E_g^2 + 8.32449E_g^3, \quad (22)$$

where  $\varepsilon_{\infty}$  oriented for high-frequency dielectric constant and  $\varepsilon_0$  referred to as the static dielectric constant. Table 4a,b provides the computation values of the  $\varepsilon_{\infty}$  and  $\varepsilon_0$  regarding their direct and indirect bandgaps of different concentrations of ZnO- doped PVA/PVP polymeric nanocomposite films. The deviation on the values is calculated where the ranging values of  $\varepsilon_{\infty}$  from 3.65 to 7.035, while for the  $\varepsilon_0$  from 467.74 to 7.045. The enhancement of ZnO dramatically falls out of the dielectric values for the proposed ZnO-doped PVA/PVP nanocomposites.

**Table 4.** The nonlinear calculated optical values for the indirect bandgap of the various systems.

<b>(a) Indirect Bandgap of the Multiple Systems.</b>					
<b>Samples</b>	<b>High-Frequency Dielectric Constants, (<math>\varepsilon_{\infty}</math>)</b>	<b>Static Dielectric Constant, (<math>\varepsilon_0</math>)</b>	<b><math>\chi^{(1)}</math> (esu)</b>	<b><math>\chi^{(3)}</math>, <math>10^{-13}</math> (esu)</b>	<b><math>n_{(2)}</math>, <math>10^{-11}</math> (esu)</b>
Pure PB ZnO <sub>0</sub>	3.83	467.74	0.225	4.41	0.848
PB ZnO <sub>1</sub>	3.96	385.101	0.235	5.26	0.996
PB ZnO <sub>2</sub>	4.12	299.072	0.2490	6.538	1.212
PB ZnO <sub>3</sub>	6.53	8.102	0.4403	63.914	9.42
PB ZnO <sub>4</sub>	7.29	7.317	0.5011	107.26	14.96
PB ZnO <sub>5</sub>	7.91	8.597	0.5502	155.85	20.87
<b>(b) Direct bandgaps of the different approaches.</b>					
Pure PB ZnO <sub>0</sub>	3.65	617.14	0.211	3.37	0.665
PB ZnO <sub>1</sub>	3.67	591.88	0.213	3.518	0.691
PB ZnO <sub>2</sub>	3.71	557.35	0.216	3.733	0.729
PB ZnO <sub>3</sub>	5.98	14.85	0.397	42.243	6.50
PB ZnO <sub>4</sub>	6.24	10.54	0.417	51.724	7.79
PB ZnO <sub>5</sub>	6.82	7.133	0.464	78.913	11.37

### 3.4. Optical Limiting Effect of ZnO-Doped PVA/PVP Nanocomposite Films

The study gains strength from including the optical limiting effect in exploring the non-linear optical properties of ZnO-doped PVA/PVP nanocomposites. The limiting effect refers to the threshold at which incoming light is restricted from accessing the films. This investigation employs two laser sources with wavelengths of 632.8 and 532 nm. In Figure 8a,b, the relationship between output power and normalized power is plotted for the two lasers as a function of the ZnO-filled PVA/PVP film's weight percentage. Interestingly, an increase in the weight percentage of ZnO leads to a decrease in output power and its corresponding normalized power (i.e., output power divided by input power), potentially caused by an uncontrolled factor defocusing the laser beam. However, adding more ZnO NPs in the host matrix shows a significant exponential reduction in the optical limiting effect. These findings suggest that the proposed ZnO-doped PVA/PVP polymeric films exhibit the potential for higher laser attenuation, thus providing solid evidence for the films' suitability in laser applications.

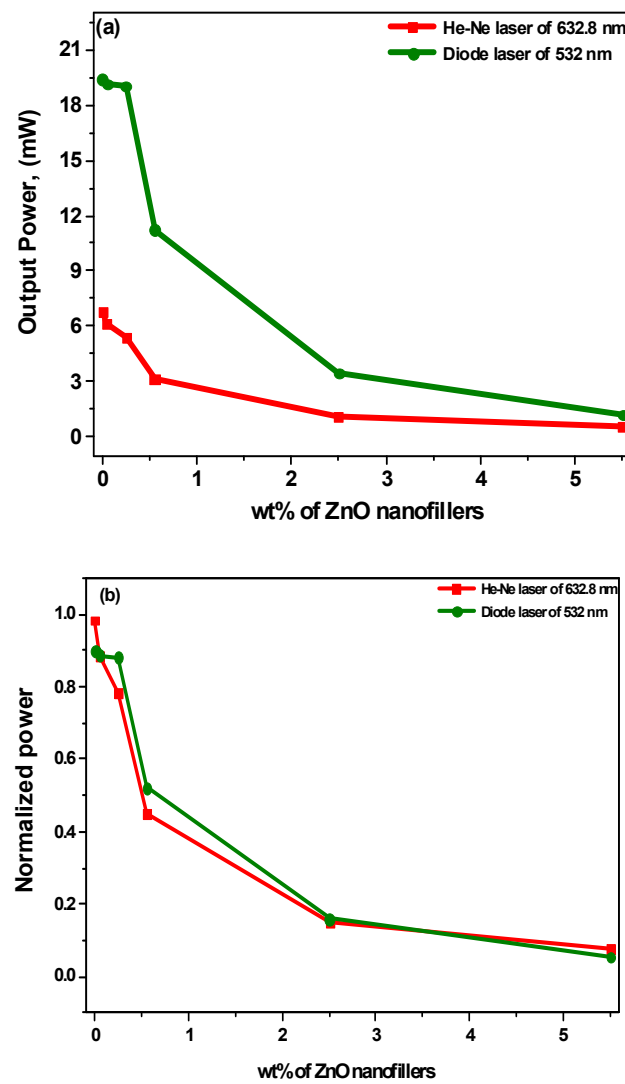


**Figure 8.** (a,b): (a) Output power, (b) Normalized power to study the optical limiting effects using two excitation sources: He-Ne laser at 638.2 nm and diode laser at 532 nm for PB ZnO nanocomposite films.

### 3.5. Dielectric Behavior of ZnO-Doped PVA/PVP Nanocomposite Films

The dielectric function is crucial in characterizing the interaction between a material and electromagnetic radiation (EM). It detects and responds to any deviations in the reaction, providing insight into the EM propagation within the material. Furthermore, the dielectric function governs the behavior and properties of nanocomposite films under AC fields by determining their derivation and nature. The relationship between the dielectric function and these films is described by a correlation reported as [88]:

$$\epsilon_r^* = \epsilon' - j\epsilon''(\omega), \quad (23)$$

$$\epsilon' = \frac{C_p \times t}{\epsilon_0 \times A}, \quad (24)$$

$$\epsilon'' = \epsilon' \tan \delta \quad (25)$$

where  $C_p$  is the parallel measured capacitance,  $t$  is the thickness of the films,  $\epsilon_0$  is the free space permittivity, and  $A$  corresponds to the area tested of the polymer under the holder electrode. Additionally,  $\epsilon'$  is accounted for by the dielectric constant; on the other

hand,  $\epsilon''$  marks for dielectric loss and  $\tan \delta$  is the tangent loss. Figure 9a–c shows the dielectric permittivity against the frequency for the ZnO-doped on the PVA/PVP blend polymer. The first interesting finding is the gradual decrease in the  $\epsilon'$  and  $\epsilon''$  as the frequency increases. The highest values of  $\epsilon'$  and  $\epsilon''$  are determined with an enhancement of ZnO on the PVA/PVP matrix. Respectively, in the low-frequency region, the inverse relation was observed with increased values of  $\epsilon'$  and  $\epsilon''$  dielectric permittivity. In contrast, a saturation of  $\epsilon'$  and  $\epsilon''$  values was observed in the high-frequency region.

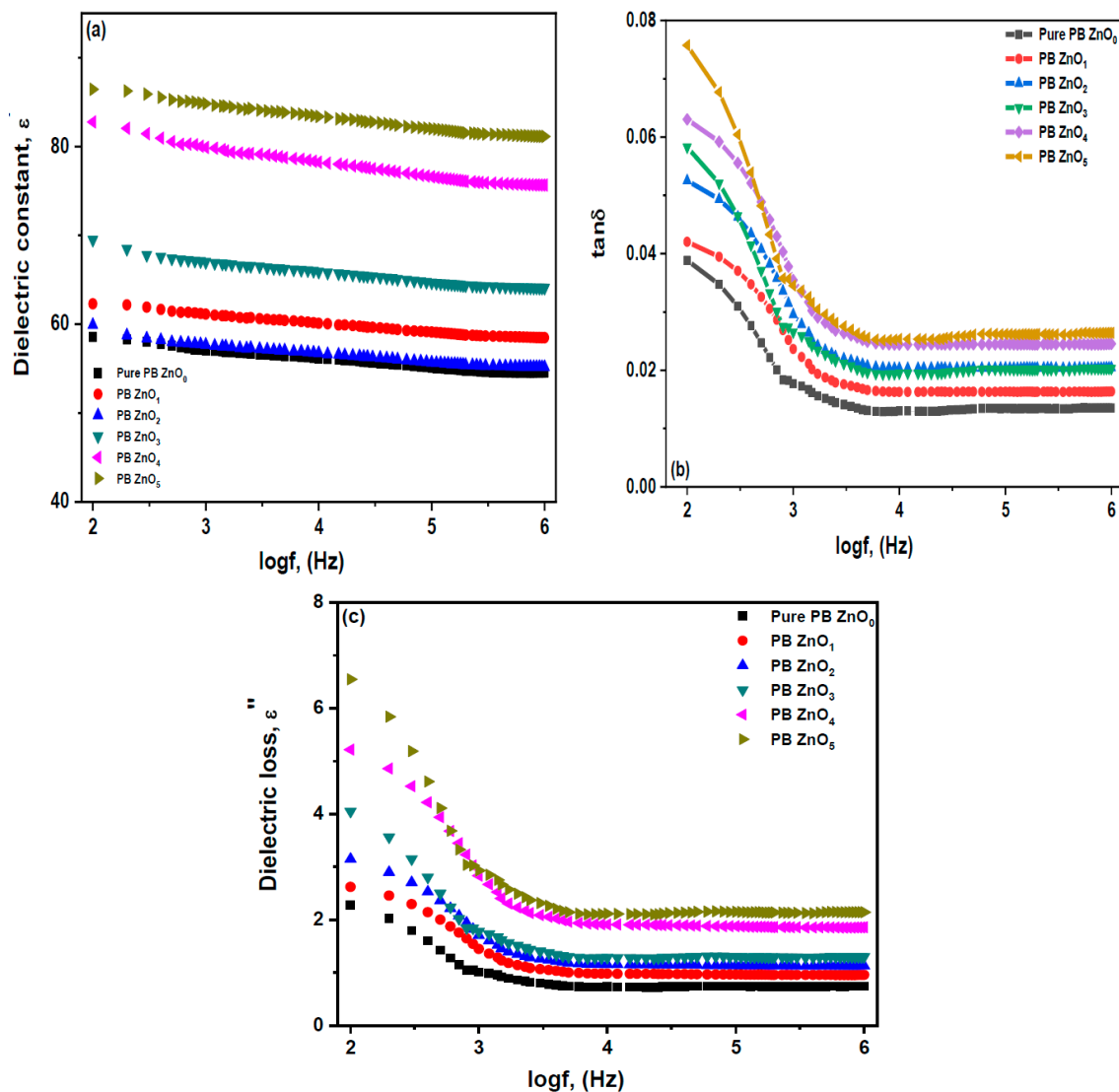


**Figure 9.** (a–c): (a) Real part of dielectric permittivity, (b)  $\tan \delta$ , and (c) imaginary part of dielectric permittivity against angular frequency for PB ZnO nanocomposite films.

Furthermore, to gain more insights into the behavior of the dielectric properties concerning the increasing values of  $\epsilon'$ , it has been observed that the provided attitude leads to an enhancement in the conductivity of the films. This is attributed to the increase in carrier concentration and mobility [81]. Additionally, the rise in  $\epsilon'$  at the lower frequency region is ascribed to the effect of polarization on the films. On the other hand, the emergence of low  $\epsilon'$  values indicates the potential of films for electronic insulation. However, the dielectric loss decreases in the high-frequency region, implying a lack of ion diffusion [62]. This is attributed to the time limit for pole molecules to recover and produce an electric field in the high-frequency area [81]. The changes in dielectric permittivities shift towards the right side for the as-prepared nanocomposite fills with ZnO NPs, and the increase

in dielectric permittivity with a high content of ZnO suggests a crucial increment in the density of the mobile ions.

Figure 9b illustrates the variation of the dielectric loss tangent for ZnO loaded in the blend polymer. The dropping of  $\tan\delta$  at the lower frequency values can be attributed to the influence of the polarization effect, which describes the decrease phenomenon. This is due to the exchange of charge transfer energy between the ZnO and the PVA/PVP blend polymer. Furthermore, the marked point with the polarization becomes more robust as the charge carrier transfers a motion, thus building a loss at a higher frequency region [89]. The reinforcement of the host matrix with numerous wt% of ZnO nanofiller causes an increase in the values of tangent loss.

In another study, the  $\epsilon'$  and  $\epsilon''$  were investigated concerning the different wt% of ZnO at 30 °C of fixed frequency from 100 Hz to 1 MHz, as depicted in Figure 10a,b. The results indicate a change in frequency units facing a decrease in dielectric permittivity values. The utmost values of  $\epsilon'$  and  $\epsilon''$  exist at a lower frequency, and ZnO with high wt% caused a linear increase in dielectric parameters. These findings result from increased charge carrier density and space charge in the blend host matrix [62]. Additionally, it is essential to note that the growth of electrode polarization leads to the disposal of any effect of high-frequency dielectric properties [90].

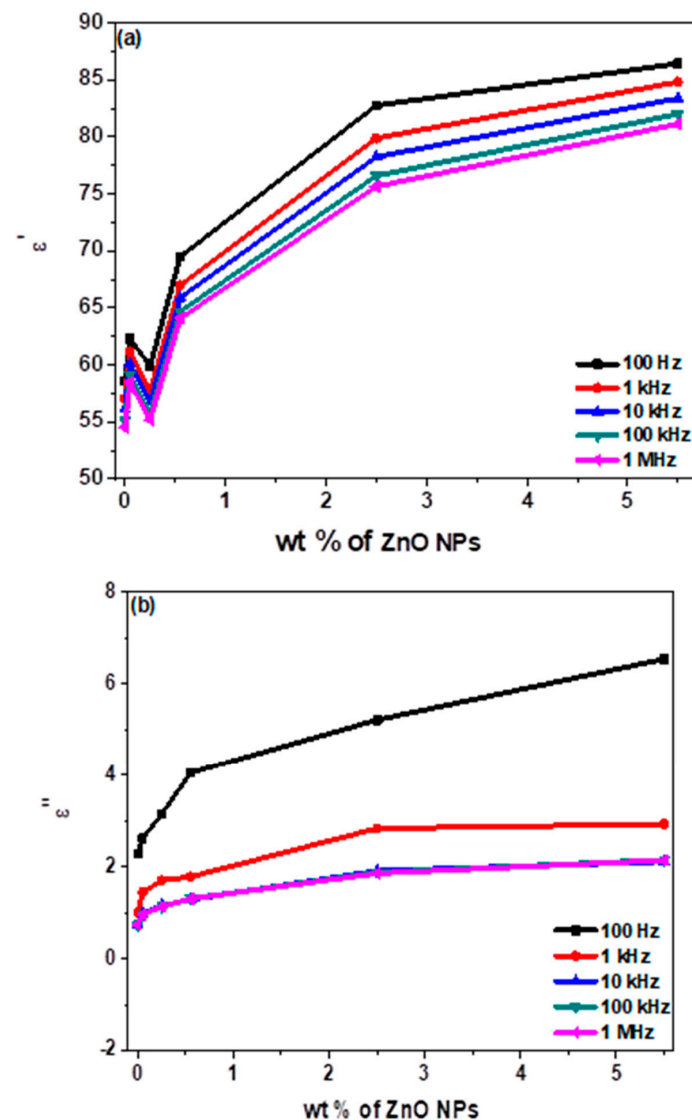


Figure 10. (a,b): Dependence of (a)  $\epsilon'$ , and (b)  $\epsilon''$  values on wt% of ZnO nanofiller at 30 °C.

### 3.6. The Electric Modules of ZnO-Doped PVA/PVP Nanocomposite Films

The investigation into the electrical properties of samples provides valuable insights into the prevalence of electrode polarization. The identification of these electrical properties is based on the dielectric data discussed in reference [91]:

$$M^* = \frac{1}{\varepsilon^*} = \frac{\varepsilon'}{\varepsilon'^2 + \varepsilon''^2} + i \frac{\varepsilon''}{\varepsilon'^2 + \varepsilon''^2} \quad (26)$$

$$M^* = M' + iM'' \quad (27)$$

Figure 11a,b pictures the real ( $M'$ ) and imaginary ( $M''$ ) modulus with applied frequency at room temperature. From Figure 11a, at the lower frequency region, the  $M'$  value seems to go toward zero as the ZnO increases inside the blend polymers. These results suggest that the materials are ruled out from any electrode polarization effect [91]. The drop of  $M'$  values and the increase of ZnO wt% affirmed the rise in electrode polarization and decrease in the resistance of the samples [92]. Although, the missing relaxation peaks on the  $M'$  compatible with  $\varepsilon'$  in complex permittivity. These findings support the material ability in  $M'$  to store energy. However, regarding the imaginary  $M''$  part of the electric modulus, the frequency increase, followed by a decrease in  $M''$  values. The reason for this is associated with the restricted distance of charge carriers. A constant attitude of  $M''$  is noticeable at a higher frequency region. The relaxation peak reported in the  $M''$  electric modulus. After the ZnO is filled with blend polymer, as the higher content of ZnO, a displacement of relaxation peaks is recorded, these may cause an increase in relaxation time and a reduction in ionic conductivity [93].

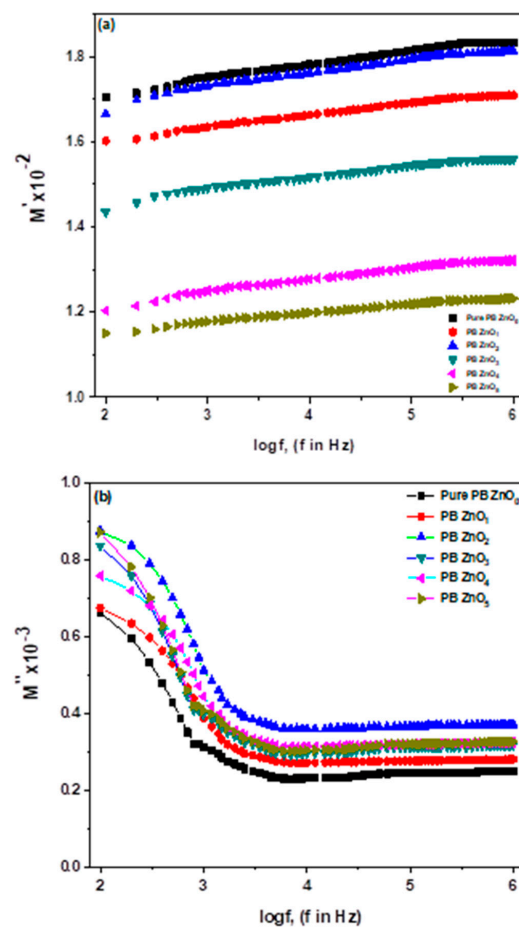


**Figure 11.** (a,b): (a) Real part of electric modulus ( $M'$ ), (b) Imaginary part of electric modulus ( $M''$ ) versus frequency for samples at room temperature.

### 3.7. AC Electrical Conductivity of ZnO-Doped PVA/PVP Nanocomposite Films

An advantage of identifying the frequency dependent on the AC electrical conductivity technique is offering information about the nanocomposite films' conduction mechanism. Therefore, to compute the AC electrical conductivity of the proposed nanocomposite films, the following equations were used [94]:

$$\sigma_{Total.AC}(\omega) = \frac{t}{ZA}, \quad (28)$$

$$\sigma_{Total.AC}(\omega) = \sigma_{DC}(\omega \rightarrow 0) + \sigma_{AC}(\omega), \quad (29)$$

$$\sigma_{AC}(\omega) = A\omega^s, \quad (30)$$

Here, the total AC electrical conductivity, named  $\sigma_{Total.AC}(\omega)$ ,  $Z$  describes the impedance, and  $A$  is the constant parameter that relies on the temperature. Moreover,  $\sigma_{DC}(\omega \rightarrow 0)$  and  $\sigma_{AC}(\omega)$  known as the terms of the AC and DC electrical conductivities, where  $\omega$  is the dependent frequency and  $s$  is the exponent frequency. The graph in Figure 12 displays the relationship between the AC electrical conductivity and frequency for a PVA/PVP polymer blend containing various percentages of ZnO. As the amount of ZnO doping increases, so does the AC conductivity, indicating a correlation between enhanced charge carrier mobility [95] and AC conductivity. The frequency-dependent AC conductivity values increase with varying ZnO doping levels in the polymer blend, leading to a rise in free ions. The AC plots were extrapolated to estimate DC electrical conductivity, and the computed values are presented in Table 5. Despite ZnO being well dispersed in the blend polymer, the conductivity values were lower, except for the PB ZnO<sub>5</sub> sample. This suggests electrode polarization could cause decreased DC values as increasing ZnO loading leads to longer polymer chains, thereby reducing DC conductivity [92]. The exponent  $s$  is a critical parameter used to describe the interactions between material impurities and charge carriers, and its value depends on temperature and frequency. The standard Debye medium is one, and the  $s$  value ranges from zero to one. Table 5 summarizes the  $s$  values of the ZnO nanocomposite films, which shifted remarkably from 1.00618 to 0.9977. The observed drop in  $s$  values with high ZnO dispersion is linked to the power law of Jonscher's [81] and is a significant predictor of increased charge carriers.

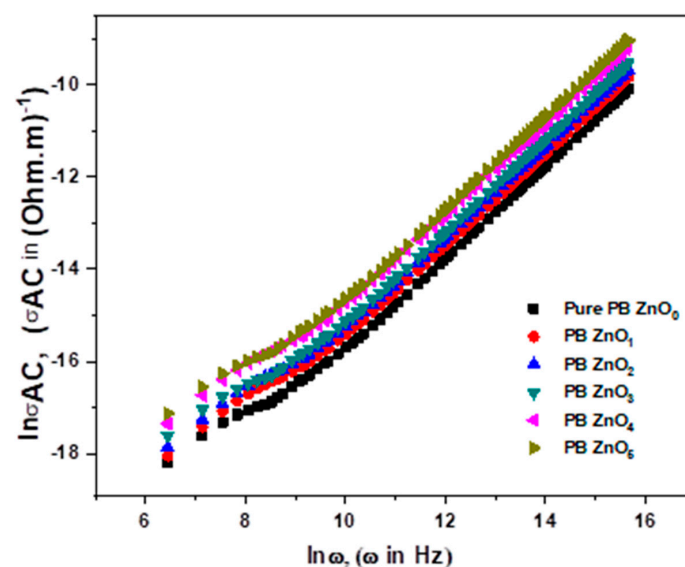


**Figure 12.** AC conductivity versus angular frequency for different systems with various wt.% of ZnO nanofillers.



**Table 5.** Values of DC electrical conductivity  $\sigma_{dc}$  determined from the lower frequency fit of  $\sigma_{ac}$  spectra to the power law and their corresponding fractional exponent  $s$ .

Samples	$\sigma_{dc}$ (S/m)	$s$
Pure PB ZnO <sub>0</sub>	$1.53 \times 10^{-8}$	1.00618
PB ZnO <sub>1</sub>	$2.68 \times 10^{-8}$	1.00576
PB ZnO <sub>2</sub>	$3.01 \times 10^{-8}$	1.00529
PB ZnO <sub>3</sub>	$3.49 \times 10^{-8}$	0.99833
PB ZnO <sub>4</sub>	$7.51 \times 10^{-8}$	0.99786
PB ZnO <sub>5</sub>	$1.76 \times 10^{-7}$	0.9977

### 3.8. Nonlinear I–V Characteristics of ZnO-Doped PVA/PVP Nanocomposite Films

The varistor plays a crucial role in electronic circuits, also known as the Voltage-Dependent Resistor (VDR), exhibiting a high nonlinearity of current-voltage characteristics. When dealing with a polymer sample, it is important to establish simplified criteria for a maximum value of  $\rho$  and a low threshold. Figure 13a–d illustrates the current-voltage (I–V) behavior of a blend polymer doped with various concentrations of ZnO. An ohmic behavior is expected at low voltages with a linear relationship between the applied voltage and electrical current. However, as the applied voltage increases, the electrical current initially increases and then accelerates at a higher rate, indicating a non-ohmic behavior.

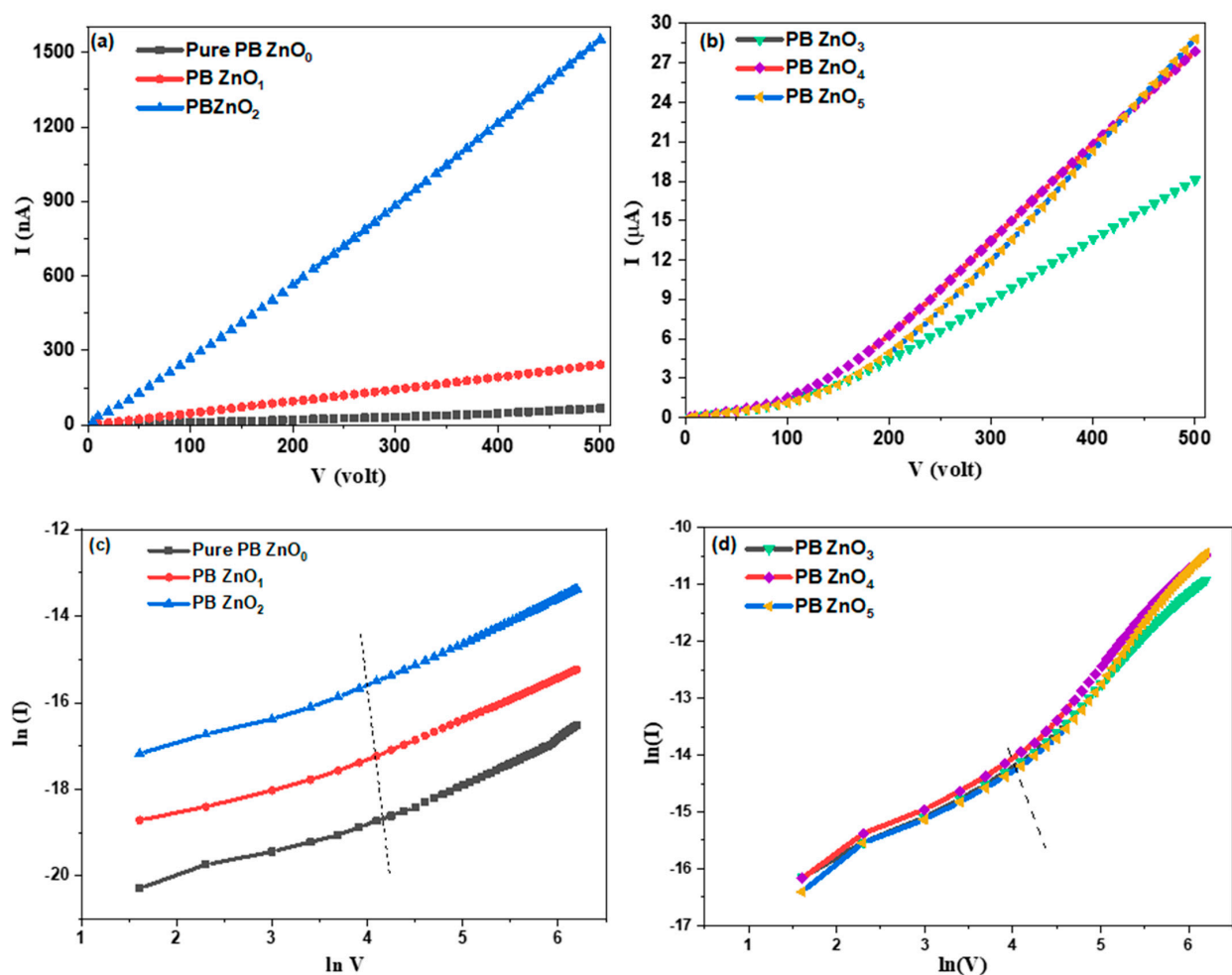


**Figure 13.** (a–d): Variation of current ( $I$ )-voltage ( $V$ ) plots and the corresponding  $\ln(I)$ - $\ln(V)$  plots of ZnO/(PVA-PVP) polymeric composite films.

Moreover, enhancing the ZnO contents in the blend polymer increases the current. However, the region of ohmic resistivity is located at the low doping contents. Therefore, the coefficient ( $\rho$ ) corresponding to the measurements of the nonlinearity of varistors is given by the following equation [96]:

$$\rho = \frac{d(\log I)}{d(\log V)} \quad (31)$$

Figure 13c,d represents the logarithm of  $I$  and  $V$  for the blend polymer doping with ZnO nanocomposite films. The slope of the nonlinear parameter is listed in Table 6. The criteria for inclusion of conduction mechanisms for all  $\rho$  values are as follows: If  $\rho = 1$ , the sample exhibits ohmic behavior, whereas if  $\rho = 2$ , the dominant mechanism is SCLC (space charge limiting current). If  $\rho > 2$ , the mechanism reported is TCL (trap charge limited) [97–99]. Three distinct regions were identified in the case of Pure PB ZnO<sub>0</sub>, PB ZnO<sub>3</sub>, PB ZnO<sub>4</sub>, and PB ZnO<sub>5</sub> samples. However, PB ZnO<sub>1</sub> and PB ZnO<sub>2</sub> samples were described with two regions. In these samples, the first region was detected close to 1, while the second region for the first two samples was close to 1 and then increased with a ratio of ZnO until it exceeded 2. The third region is currently close to 1. The  $\rho$  value near 1 is attributed to the symmetry of the ohmic resistivity behavior. Furthermore, adding high ZnO content can shift the I-V characteristics to a higher applied voltage, decreasing the sample's resistance. The high doping of ZnO causes the formation of a gap at the base of the films, allowing many charges to transfer between levels as the electric current values increase from nA to mA at higher applied voltage. Therefore, incorporating ZnO into the polymer blend can facilitate the development of novel and more cost-effective varistors.

**Table 6.** The values of nonlinear exponent parameters for the ZnO doped in blend polymer.

Sample	$\rho_1$	$\rho_2$	$\rho_3$
Pure PB ZnO <sub>0</sub>	0.57	0.97	1.60
PB ZnO <sub>1</sub>	0.54	0.94	
PB ZnO <sub>2</sub>	0.60	1.01	
PB ZnO <sub>3</sub>	0.97	1.61	1.44
PB ZnO <sub>4</sub>	0.86	1.87	1.41
PB ZnO <sub>5</sub>	0.87	2.04	1.68

#### 4. Conclusions

The solution casting technique provides a cost-effective and efficient means of preparing high-quality ZnO-doped PVA/PVP films. The semicrystalline nature of the PVA/PVP blend is revealed through X-ray diffraction (XRD) analysis. The effect of ZnO doping is investigated through Fourier-transform infrared spectroscopy (FT-IR) analysis, while the paper extensively discusses optical properties. The absorption spectra show surface plasmon resonance (SPR), and the bandgap energy obtained through both Tauc's and Amorphous Semiconductor Model ASF is found to decrease as the nanofiller content increases in the blend polymer. The refractive index/bandgap relationship is described using the variable of a semiempirical equation. The ZnO doping level in the blend polymer affects the nonlinear optical parameters. Interaction between ZnO and the blend matrix is inferred from the disappearance of the relaxation peak on the  $M''$  of electric modulus at lower-frequency regions. The AC electrical conductivity and dielectric permittivity parameters increase with higher ZnO weight percentages. The nonlinear I-V characteristics show three possible regions, and linear relationships are observed between the applied voltage and electrical current. Overall, the ZnO-doped PVA/PVP films show promising potential for future development in electronic devices, nonlinear optics, laser cut-off filters, and varistor applications.

**Author Contributions:** T.H.A.: Writing—Review, and Methodology. A.A.: Methodology, and Software. M.S.A.: Review data, and Data curation. F.A.H.: Formal analysis, and Software. M.S.A.-A.: Visualization, and Methodology. I.S.Y.: Visualization, Methodology, and Supervision. H.Y.Z.: Writing original draft, and Formal analysis. M.I.M.: Visualization, and Methodology. S.H.Z.: Software, and Data curation. M.S.A.-w.: Methodology, Formal analysis, and Writing original draft. All authors have read and agreed to the published version of the manuscript.

**Funding:** The authors would like to acknowledge the support of the Ministry of Education, Kingdom of Saudi Arabia, for this research through a grant (PCSED-020-18) under the Promising Centre for Sensors and Electronic Devices (PCSED) at Najran University, Kingdom of Saudi Arabia. The Research Center for Advanced Materials Science (RCAMS) at King Khalid University, Saudi Arabia, for funding this work under the grant number RCAMS/KKU/017-22. Additionally, the authors would like to thank the Deanship of Graduate Studies and Research, Ajman University, Ajman, UAE for the financial assistance through Grant number (Project ID, DGSR Ref. Number: 2022-IRG-HBS-1).

**Data Availability Statement:** Data are contained within the article.

**Conflicts of Interest:** The authors declare no conflict of interest.

## References

- Burleigh, T.D.; Ruhe, C.; Forsyth, J. Photo-Corrosion of Different Metals during Long-Term Exposure to Ultraviolet Light. *Corrosion* **2003**, *59*, 774–779. [CrossRef]
- Ahn, J.H.; Bertoni, C.; Dunn, S.; Wang, C.; Talapin, D.V.; Gaponik, N.; Eychmüller, A.; Hua, Y.; Bryce, M.R.; Petty, M.C. White organic light-emitting devices incorporating nanoparticles of II–VI semiconductors. *Nanotechnology* **2007**, *18*, 33. [CrossRef]
- Kurchatov, I.S.; Bulychev, N.A.; Bundyuk, A.V.; Kazaryan, M.A.; Kustov, D.M. Study of spectral characteristics of materials for IR lasers based on II–VI semiconductors doped with iron-group ions. *Bull. Lebedev Phys. Inst.* **2015**, *42*, 107–109. [CrossRef]
- Trivedi, S.B.; Wang, C.-C.; Kutcher, S.; Hommerich, U.; Palosz, W. Crystal growth technology of binary and ternary II–VI semiconductors for photonic applications. *J. Cryst. Growth* **2007**, *310*, 1099–1106. [CrossRef]
- Weickmann, H.; Tiller, J.C.; Thomann, R.; Mülhaupt, R. Metallized Organoclays as New Intermediates for Aqueous Nanohybrid Dispersions, Nanohybrid Catalysts and Antimicrobial Polymer Hybrid Nanocomposites. *Macromol. Mater. Eng.* **2005**, *290*, 875–883. [CrossRef]
- Hassan, N.K.; Hashim, M.R.; Al-Douri, Y.; Al-Heuseen, K. Current Dependence Growth of ZnO Nanostructures by Electrochemical Deposition Technique. *Int. J. Electrochem. Sci.* **2012**, *7*, 4625–4635.
- Ali, A.M.; Harraz, F.A.; Ismail, A.A.; Al-Sayari, S.; Algarni, H.; Al-Sehemi, A.G. Synthesis of amorphous ZnO–SiO<sub>2</sub> nanocomposite with enhanced chemical sensing properties. *Thin Solid Films* **2016**, *605*, 277–282. [CrossRef]
- Jeeju, P.; Jayalekshmi, S.; Chandrasekharan, K.; Sudheesh, P. Enhanced linear and nonlinear optical properties of thermally stable ZnO/poly(styrene)–poly(methyl methacrylate) nanocomposite films. *Thin Solid Films* **2013**, *531*, 378–384. [CrossRef]
- Kumar, S.; Krishnakumar, B.; Sobral, A.J.; Koh, J. Bio-based (chitosan/PVA/ZnO) nanocomposites film: Thermally stable and photoluminescence material for removal of organic dye. *Carbohydr. Polym.* **2018**, *205*, 559–564. [CrossRef]
- Dincă, V.; Mocanu, A.; Isopencu, G.; Busuioc, C.; Brajnicov, S.; Vlad, A.; Icriverzi, M.; Roseanu, A.; Dinescu, M.; Stroescu, M.; et al. Biocompatible pure ZnO nanoparticles-3D bacterial cellulose biointerfaces with antibacterial properties. *Arab. J. Chem.* **2018**, *13*, 3521–3533. [CrossRef]
- Zhang, D.; Chava, S.; Berven, C.; Lee, S.K.; Devitt, R.; Katkanant, V. Experimental study of electrical properties of ZnO nanowire random networks for gas sensing and electronic devices. *Appl. Phys. A* **2010**, *100*, 145–150. [CrossRef]
- Lee, C.-T. Fabrication Methods and Luminescent Properties of ZnO Materials for Light-Emitting Diodes. *Materials* **2010**, *3*, 2218–2259. [CrossRef]
- Ghorai, A.; Bayan, S.; Gogurla, N.; Midya, A.; Ray, S.K. Highly Luminescent WS<sub>2</sub> Quantum Dots/ZnO Heterojunctions for Light Emitting Devices. *ACS Appl. Mater. Interfaces* **2016**, *9*, 558–565. [CrossRef]
- Wang, H.; Cao, S.; Yang, B.; Li, H.; Wang, M.; Hu, X.; Sun, K.; Zang, Z. NH<sub>4</sub> Cl-Modified ZnO for High-Performance CsPbIBr<sub>2</sub> Perovskite Solar Cells via Low-Temperature Process. *Sol. RRL* **2020**, *4*, 1900363. [CrossRef]
- Nanosized ZnO Prepared by Homogeneous Precipitation and Its Photocatalytic Property | Request PDF n.d. Available online: [https://www.researchgate.net/publication/284381907\\_Nanosized\\_ZnO\\_prepared\\_by\\_homogeneous\\_precipitation\\_and\\_its\\_photocatalytic\\_property?msclid=69250a7bcf4011ecb776c632f4231966](https://www.researchgate.net/publication/284381907_Nanosized_ZnO_prepared_by_homogeneous_precipitation_and_its_photocatalytic_property?msclid=69250a7bcf4011ecb776c632f4231966) (accessed on 9 May 2022).
- Zhao, X.; Zheng, B.; Li, C.; Gu, H. Acetate-derived ZnO ultrafine particles synthesized by spray pyrolysis. *Powder Technol.* **1998**, *100*, 20–23. [CrossRef]
- Damonte, L.; Zélis, L.M.; Soucase, B.M.; Fenollosa, M.H. Nanoparticles of ZnO obtained by mechanical milling. *Powder Technol.* **2004**, *148*, 15–19. [CrossRef]
- Venkatachalam, S. Ultraviolet and visible spectroscopy studies of nanofillers and their polymer nanocomposites. In *Spectroscopy of Polymer Nanocomposites*; Thomas, S., Rouxel, D., Ponnamm, D., Eds.; William Andrew: New York, NY, USA, 2016; pp. 130–157. [CrossRef]

19. Wen, F.; Zhu, C.; Li, L.; Zhou, B.; Zhang, L.; Han, C.; Li, W.; Yue, Z.; Wu, W.; Wang, G.; et al. Enhanced energy storage performance of polymer nanocomposites using hybrid 2D ZnO@MoS<sub>2</sub> semiconductive nano-fillers. *Chem. Eng. J.* **2021**, *430*, 132676. [\[CrossRef\]](#)
20. Wang, N.; Yu, J.; Ma, X. Preparation and characterization of compatible thermoplastic dry starch/poly(lactic acid). *Polym. Compos.* **2008**, *29*, 551–559. [\[CrossRef\]](#)
21. Tucureanu, V.; Matei, A.; Mihalache, I.; Danila, M.; Popescu, M.; Bitu, B. Synthesis and characterization of YAG:Ce,Gd and YAG:Ce,Gd/PMMA nanocomposites for optoelectronic applications. *J. Mater. Sci.* **2014**, *50*, 1883–1890. [\[CrossRef\]](#)
22. Subbu, C.; Rajendran, S.; Kesavan, K.; Premila, R. The physical and electrochemical properties of poly(vinylidene chloride-co-acrylonitrile)-based polymer electrolytes prepared with different plasticizers. *Ionics* **2015**, *22*, 229–240. [\[CrossRef\]](#)
23. Su, F.-H.; Zhang, Z.-Z. Friction and wear behavior of glass fabric/phenolic resin composites with surface-modified glass fabric. *J. Appl. Polym. Sci.* **2009**, *112*, 594–601. [\[CrossRef\]](#)
24. Liao, C.Z.; Bao, S.P.; Tjong, S.C. Microstructure and fracture behavior of maleated high-density polyethylene/silicon carbide nanocomposites toughened with poly(styrene-ethylene-butylene-styrene) triblock copolymer. *Adv. Polym. Technol.* **2011**, *30*, 322–333. [\[CrossRef\]](#)
25. Nicho, M.; García-Escobar, C.; Arenas, M.; Altuzar-Coello, P.; Cruz-Silva, R.; Güizado-Rodríguez, M. Influence of P3HT concentration on morphological, optical and electrical properties of P3HT/PS and P3HT/PMMA binary blends. *Mater. Sci. Eng. B* **2011**, *176*, 1393–1400. [\[CrossRef\]](#)
26. Deghiedy, N.; El-Sayed, S. Evaluation of the structural and optical characters of PVA/PVP blended films. *Opt. Mater.* **2020**, *100*, 109667. [\[CrossRef\]](#)
27. Saad, M.; Husain, B. Synthesis of PVA/PVP Based Hydrogel for Biomedical Applications: A Review. *Energy Sources Part A* **2018**, *40*, 2388–2393. [\[CrossRef\]](#)
28. Zidan, H.M.; Abdelrazek, E.M.; Abdelghany, A.M.; Tarabiah, A.E. Characterization and some physical studies of PVA/PVP filled with MWCNTs. *J. Mater. Res. Technol.* **2018**, *8*, 904–913. [\[CrossRef\]](#)
29. Gaaz, T.S.; Sulong, A.B.; Akhtar, M.N.; Kadhum, A.A.H.; Mohamad, A.B.; Al-Amiery, A.A. Properties and Applications of Polyvinyl Alcohol, Halloysite Nanotubes and Their Nanocomposites. *Molecules* **2015**, *20*, 22833–22847. [\[CrossRef\]](#)
30. Hussein, S.I.; Abd-Elnaïem, A.M.; Ali, N.A.; Mebed, A.M. Enhanced Thermo-Mechanical Properties of Poly(vinyl alcohol)/Poly(vinyl pyrrolidone) Polymer Blended with Nanographene. *Curr. Nanosci.* **2020**, *16*, 994–1001. [\[CrossRef\]](#)
31. Cassu, S.N.; Felisberti, M.I. Poly(vinyl alcohol) and poly(vinyl pyrrolidone) blends: Miscibility, microheterogeneity and free volume change. *Polymer* **1997**, *38*, 3907–3911. [\[CrossRef\]](#)
32. El Salmawi, K.M. Gamma Radiation-Induced Crosslinked PVA/Chitosan Blends for Wound Dressing. *J. Macromol. Sci. Part A* **2007**, *44*, 541–545. [\[CrossRef\]](#)
33. Ma, R.; Xiong, D.; Miao, F.; Zhang, J.; Peng, Y. Novel PVP/PVA hydrogels for articular cartilage replacement. *Mater. Sci. Eng. C* **2009**, *29*, 1979–1983. [\[CrossRef\]](#)
34. Tang, S.; Murto, P.; Wang, J.; Larsen, C.; Andersson, M.R.; Wang, E.; Edman, L. On the Design of Host–Guest Light-Emitting Electrochemical Cells: Should the Guest be Physically Blended or Chemically Incorporated into the Host for Efficient Emission? *Adv. Opt. Mater.* **2019**, *7*, 1900451. [\[CrossRef\]](#)
35. Baeg, K.-J.; Caironi, M.; Noh, Y.-Y. Toward Printed Integrated Circuits based on Unipolar or Ambipolar Polymer Semiconductors. *Adv. Mater.* **2013**, *25*, 4210–4244. [\[CrossRef\]](#) [\[PubMed\]](#)
36. Kavitha, B.; Sekhar, K.C.; Kumar, K.S.; Narsimlu, N. Influence of NaBr on Structural Studies of PVA/TiO<sub>2</sub> Polymer Composites. *Optik* **2023**, *272*, 170244. [\[CrossRef\]](#)
37. Pasha, S.K.K.; Deshmukh, K.; Ahamed, M.B.; Chidambaram, K.; Mohanapriya, M.K.; Raj, N.A.N. Investigation of Microstructure, Morphology, Mechanical, and Dielectric Properties of PVA/PbO Nanocomposites. *Adv. Polym. Technol.* **2015**, *36*, 352–361. [\[CrossRef\]](#)
38. Ramesan, M.T. Synthesis and Characterization of Magnetoelectric Nanomaterial Composed of Fe<sub>3</sub>O<sub>4</sub> and Polyindole. *Adv. Polym. Technol.* **2013**, *32*, 21362. [\[CrossRef\]](#)
39. Choudhary, S.; Sengwa, R. ZnO nanoparticles dispersed PVA–PVP blend matrix based high performance flexible nanodielectrics for multifunctional microelectronic devices. *Curr. Appl. Phys.* **2018**, *18*, 1041–1058. [\[CrossRef\]](#)
40. Ramesan, M.T.; Varghese, M.; Jayakrishnan, P.; Periyat, P. Silver-Doped Zinc Oxide as a Nanofiller for Development of Poly(vinyl alcohol)/Poly(vinyl pyrrolidone) Blend Nanocomposites. *Adv. Polym. Technol.* **2016**, *37*, 137–143. [\[CrossRef\]](#)
41. Ahangar, E.G.; Abbaspour-Fard, M.H.; Shahtahmassebi, N.; Khojastehpour, M.; Maddahi, P. Preparation and Characterization of PVA/ZnO Nanocomposite. *J. Food Process. Preserv.* **2014**, *39*, 1442–1451. [\[CrossRef\]](#)
42. Alghunaim, N.S.; Alhusaiki-Alghamdi, H. Role of ZnO nanoparticles on the structural, optical and dielectric properties of PVP/PC blend. *Phys. B Condens. Matter* **2019**, *560*, 185–190. [\[CrossRef\]](#)
43. Ali, F.; Kershi, R.; Sayed, M.; AbouDeif, Y. Evaluation of structural and optical properties of Ce<sup>3+</sup> ions doped (PVA/PVP) composite films for new organic semiconductors. *Phys. B Condens. Matter* **2018**, *538*, 160–166. [\[CrossRef\]](#)
44. Yedurkar, S.; Maurya, C.; Mahanwar, P. Biosynthesis of Zinc Oxide Nanoparticles Using *Ixora Coccinea* Leaf Extract—A Green Approach. *Open J. Synth. Theory Appl.* **2016**, *5*, 1–14. [\[CrossRef\]](#)
45. Bigdeli, F.; Morsali, A.; Retailleau, P. Syntheses and characterization of different zinc(II) oxide nano-structures from direct thermal decomposition of 1D coordination polymers. *Polyhedron* **2010**, *29*, 801–806. [\[CrossRef\]](#)



46. Klug, H.P.; Alexander, L.E. *X-ray Diffraction Procedures: For Polycrystalline and Amorphous Materials*, 2nd ed.; Springer: Berlin, Germany, 1974; p. 992.
47. Lindon, J.C.; Tranter, G.E.; Koppenaal, D.W. *Encyclopedia of Spectroscopy and Spectrometry*, 2nd ed.; Elsevier: London, UK, 2010; Volume 3, p. 3246.
48. Williamson, G.K.; Smallman, R.E., III. Dislocation densities in some annealed and cold-worked metals from measurements on the X-ray debye-scherrer spectrum. *Philos. Mag.* **1956**, *1*, 34–46. [\[CrossRef\]](#)
49. Sadhasivam, T.; Hudson, M.S.L.; Pandey, S.K.; Bhatnagar, A.; Singh, M.K.; Gurunathan, K.; Srivastava, O. Effects of nano size mischmetal and its oxide on improving the hydrogen sorption behaviour of MgH<sub>2</sub>. *Int. J. Hydrogen Energy* **2013**, *38*, 7353–7362. [\[CrossRef\]](#)
50. Bhargava, R.N.; Gallagher, D.; Hong, X.; Nurmikko, A. Optical properties of manganese-doped nanocrystals of ZnS. *Phys. Rev. Lett.* **1994**, *72*, 416–419. [\[CrossRef\]](#)
51. Factori, I.M.; Amaral, J.M.; Camani, P.H.; Rosa, D.S.; Lima, B.A.; Brocchi, M.; da Silva, E.R.; Souza, J.S. ZnO Nanoparticle/Poly(vinyl alcohol) Nanocomposites via Microwave-Assisted Sol–Gel Synthesis for Structural Materials, UV Shielding, and Antimicrobial Activity. *ACS Appl. Nano Mater.* **2021**, *4*, 7371–7383. [\[CrossRef\]](#)
52. Dhahri, I.; Ellouze, M.; Labidi, S.; Al-Bataineh, Q.M.; Etzkorn, J.; Guermazi, H.; Telfah, A.; Tavares, C.J.; Hergenröder, R.; Appel, T. Optical and structural properties of ZnO NPs and ZnO–Bi<sub>2</sub>O<sub>3</sub> nanocomposites. *Ceram. Int.* **2021**, *48*, 266–277. [\[CrossRef\]](#)
53. Heiba, Z.K.; El-naggar, A.M.; Mohamed, M.B.; Altowairqi, Y.; Kamal, A.M. Novel Properties of PVA/PVP Polymer Blend Doped by Nano-ZnO/M (M = Co, Cu, Mn, V). *Appl. Phys. A Mater. Sci. Process.* **2021**, *127*, 1–12. [\[CrossRef\]](#)
54. Bhajantri, R.; Ravindrachary, V.; Poojary, B.; Ismayil; Harisha, A.; Crasta, V. Studies on fluorescent PVA + PVP + MPDMAPP composite films. *Polym. Eng. Sci.* **2009**, *49*, 903–909. [\[CrossRef\]](#)
55. Parameswaran, V.; Nallamuthu, N.; Devendran, P.; Manikandan, A.; Nagarajan, E.R. Assimilation of NH<sub>4</sub>Br in Polyvinyl Alcohol/Poly(N-vinyl pyrrolidone) Polymer Blend-Based Electrolyte and Its Effect on Ionic Conductivity. *J. Nanosci. Nanotechnol.* **2018**, *18*, 3944–3953. [\[CrossRef\]](#) [\[PubMed\]](#)
56. Rajendran, S.; Sivakumar, M.; Subadevi, R. Investigations on the effect of various plasticizers in PVA–PMMA solid polymer blend electrolytes. *Mater. Lett.* **2004**, *58*, 641–649. [\[CrossRef\]](#)
57. Roy, A.S.; Gupta, S.; Sindhu, S.; Parveen, A.; Ramamurthy, P.C. Dielectric properties of novel PVA/ZnO hybrid nanocomposite films. *Compos. Part B Eng.* **2013**, *47*, 314–319. [\[CrossRef\]](#)
58. Zyoud, S.H.; Almoadi, A.; AlAbdulaal, T.H.; Alqahtani, M.S.; Harraz, F.A.; Al-Assiri, M.S.; Yahia, I.S.; Zahran, H.Y.; Mohammed, M.I.; Abdel-wahab, M.S. Structural, Optical, and Electrical Investigations of Nd<sub>2</sub>O<sub>3</sub>-Doped PVA/PVP Polymeric Composites for Electronic and Optoelectronic Applications. *Polymers* **2023**, *15*, 1351. [\[CrossRef\]](#)
59. Alsaad, A.M.; Al Dairy, A.R.; Ahmad, A.A.; Al-Anbar, A.S.; Al-Bataineh, Q.M. Synthesis and characterization of as-grown doped polymerized (PMMA-PVA)/ZnO NPs hybrid thin films. *Polym. Bull.* **2021**, *79*, 2019–2040. [\[CrossRef\]](#)
60. Elhosiny Ali, H.; Abdel-Aziz, M.; Mahmoud Ibrahim, A.; Sayed, M.A.; Abd-Rabboh, H.S.; Awwad, N.S.; Algarni, H.; Shkir, M.; Yasmin Khairy, M. Microstructure Study and Linear/Nonlinear Optical Properties of Bi-Embedded PVP/PVA Films for Optoelectronic and Optical CUT-OFF Applications. *Polymers* **2022**, *14*, 1741. [\[CrossRef\]](#)
61. Aga; Mu. Doping of Polymers with ZnO Nanostructures for Optoelectronic and Sensor Applications. *Nanowires Sci. Technol.* **2010**, *2*, 205–222. [\[CrossRef\]](#)
62. Mohammed, M.I.; Khafagy, R.M.; Hussien, M.S.A.; Sakr, G.B.; Ibrahim, M.A.; Yahia, I.S.; Zahran, H.Y. Enhancing the structural, optical, electrical, properties and photocatalytic applications of ZnO/PMMA nanocomposite membranes: Towards multifunctional membranes. *J. Mater. Sci. Mater. Electron.* **2021**, *33*, 1977–2002. [\[CrossRef\]](#)
63. Im, Y.M.; Oh, T.H.; Nathanael, J.A.; Jang, S.S. Effect of ZnO nanoparticles morphology on UV blocking of poly(vinyl alcohol)/ZnO composite nanofibers. *Mater. Lett.* **2015**, *147*, 20–24. [\[CrossRef\]](#)
64. Bajpai, S.; Jadaun, M.; Tiwari, S. Synthesis, characterization and antimicrobial applications of zinc oxide nanoparticles loaded gum acacia/poly(SA) hydrogels. *Carbohydr. Polym.* **2016**, *153*, 60–65. [\[CrossRef\]](#)
65. Shanshool, H.M.; Yahaya, M.; Yunus, W.M.M.; Abdullah, I.Y. Third order nonlinearity of PMMA/ZnO nanocomposites as foils. *Opt. Quantum Electron.* **2015**, *48*, 7. [\[CrossRef\]](#)
66. Yahia, I.S.; Jilani, A.; Abutalib, M.M.; Alfaify, S.; Shkir, M.; Abdel-Wahab, M.S.; Al-Ghamdi, A.A.; El-Naggar, A.M. A Study on Linear and Non-Linear Optical Constants of Rhodamine B Thin Film Deposited on FTO Glass. *Phys. B Condens. Matter* **2016**, *490*, 25–30. [\[CrossRef\]](#)
67. Nwanya, A.; Chigbo, C.; Ezugwu, S.; Osuji, R.; Malik, M.; Ezema, F. Transformation of cadmium hydroxide to cadmium oxide thin films synthesized by SILAR deposition process: Role of varying deposition cycles. *J. Assoc. Arab. Univ. Basic Appl. Sci.* **2016**, *20*, 49–54. [\[CrossRef\]](#)
68. Muhammad, F.F.; Aziz, S.; Hussein, S.A. Effect of the dopant salt on the optical parameters of PVA:NaNO<sub>3</sub> solid polymer electrolyte. *J. Mater. Sci. Mater. Electron.* **2014**, *26*, 521–529. [\[CrossRef\]](#)
69. AlAbdulaal, T.H.; Ali, H.E.; Ganesh, V.; Aboraia, A.M.; Khairy, Y.; Hegazy, H.H.; Soldatov, A.V.; Zahran, H.Y.; Abdel-wahab, M.S.; Yahia, I.S. Investigating NaIO<sub>3</sub> Doped PVA Polymeric Nanocomposites via the Structural Morphology and Linear and Nonlinear Optical Analysis: For Optoelectronic Systems. *Optik* **2021**, *245*, 167724. [\[CrossRef\]](#)

70. Aziz, S.B.; Hassan, A.Q.; Mohammed, S.J.; Karim, W.O.; Kadir, M.F.Z.; Tajuddin, H.A.; Chan, N.N.M.Y. Structural and Optical Characteristics of PVA:C-Dot Composites: Tuning the Absorption of Ultra Violet (UV) Region. *Nanomaterials* **2019**, *9*, 216. [\[CrossRef\]](#) [\[PubMed\]](#)
71. Yassin, A.Y.; Mohamed, A.-R.; Abdelrazek, E.M.; Morsi, M.A.; Abdelghany, A. Structural investigation and enhancement of optical, electrical and thermal properties of poly (vinyl chloride-co-vinyl acetate-co-2-hydroxypropyl acrylate)/graphene oxide nanocomposites. *J. Mater. Res. Technol.* **2018**, *8*, 1111–1120. [\[CrossRef\]](#)
72. Khairy, Y.; Abdel-Aziz, M.M.; Algarni, H.; Alshehri, A.M.; Yahia, I.S.; Ali, H.E. The optical characteristic of PVA composite films doped by ZrO<sub>2</sub> for optoelectronic and block UV-Visible applications. *Mater. Res. Express* **2019**, *6*, 115346. [\[CrossRef\]](#)
73. Souri, D.; Shomalian, K. Band gap determination by absorption spectrum fitting method (ASF) and structural properties of different compositions of (60–x) V<sub>2</sub>O<sub>5</sub>–40TeO<sub>2</sub>–xSb<sub>2</sub>O<sub>3</sub> glasses. *J. Non-Crystalline Solids* **2009**, *355*, 1597–1601. [\[CrossRef\]](#)
74. Moss, T.S. Relations between the Refractive Index and Energy Gap of Semiconductors. *Phys. Status Solidi (b)* **1985**, *131*, 415–427. [\[CrossRef\]](#)
75. Ravindra, N.M.; Auluck, S.; Srivastava, V.K. On the Penn Gap in Semiconductors. *Phys. Status Solidi (b)* **1979**, *93*, K155–K160. [\[CrossRef\]](#)
76. Hervé, P.; Vandamme, L. General relation between refractive index and energy gap in semiconductors. *Infrared Phys. Technol.* **1994**, *35*, 609–615. [\[CrossRef\]](#)
77. Reddy, R.R.; Anjaneyulu, S. Analysis of the Moss and Ravindra relations. *Phys. Status Solidi (b)* **1992**, *174*, K91–K93. [\[CrossRef\]](#)
78. Anani, M.; Mathieu, C.; Lebid, S.; Amar, Y.; Chama, Z.; Abid, H. Model for calculating the refractive index of a III–V semiconductor. *Comput. Mater. Sci.* **2007**, *41*, 570–575. [\[CrossRef\]](#)
79. Kumar, V.; Singh, J.K. Model for calculating the refractive index of different materials. *Indian J. Pure Appl. Phys.* **2010**, *48*, 571–574.
80. Gomaa, H.M.; Yahia, I.; Zahran, H. Correlation between the static refractive index and the optical bandgap: Review and new empirical approach. *Phys. B Condens. Matter* **2021**, *620*, 413246. [\[CrossRef\]](#)
81. Mohammed, M.I.; Bouzidi, A.; Zahran, H.Y.; Jalalah, M.; Harraz, F.A.; Yahia, I.S. Ammonium iodide salt-doped polyvinyl alcohol polymeric electrolyte for UV-shielding filters: Synthesis, optical and dielectric characteristics. *J. Mater. Sci. Mater. Electron.* **2021**, *32*, 4416–4436. [\[CrossRef\]](#)
82. Frumar, M.; Jedelský, J.; Frumarová, B.; Wágner, T.; Hrdlička, M. Optically and thermally induced changes of structure, linear and non-linear optical properties of chalcogenides thin films. *J. Non-Crystalline Solids* **2003**, *326–327*, 399–404. [\[CrossRef\]](#)
83. Xia, J.; Liu, Y.; Qiu, X.; Mao, Y.; He, J.; Chen, L. Solvothermal synthesis of nanostructured CuInS<sub>2</sub> thin films on FTO substrates and their photoelectrochemical properties. *Mater. Chem. Phys.* **2012**, *136*, 823–830. [\[CrossRef\]](#)
84. Ticha, H.; Mater, L. Semiempirical Relation between Non-Linear Susceptibility (Refractive Index), Linear Refractive Index and Optical Gap and Its Application to Amorphous Chalcogenides. *J. Optoelectron. Adv. Mater.* **2002**, *4*, 381–386.
85. Mohammedi, A.; Ibrir, M.; Meglali, O.; Berri, S. Influence of Cu-Doping on Linear and Nonlinear Optical Properties of High-Quality ZnO Thin Films Obtained by Spin-Coating Technique. *Phys. Status Solidi (b)* **2021**, *258*, 2000472. [\[CrossRef\]](#)
86. Abutalib, M.; Yahia, I. Analysis of the linear/nonlinear optical properties of basic fuchsin dye/FTO films: Controlling the laser power of red/green lasers. *Optik* **2018**, *179*, 145–153. [\[CrossRef\]](#)
87. Jilani, W.; Bouzidi, A.; Almahri, A.; Guermazi, H.; Yahia, I.S. The effect of the thickness on structural, optical limiting, and dielectric properties of hybrid coatings rhodamine B dye films on an epoxy polymeric substrate for display applications. *Phys. Scr.* **2021**, *96*, 125862. [\[CrossRef\]](#)
88. Choudhary, S. Structural, optical, dielectric and electrical properties of (PEO–PVP)–ZnO nanocomposites. *J. Phys. Chem. Solids* **2018**, *121*, 196–209. [\[CrossRef\]](#)
89. Hemalatha, K.; Rukmani, K. Concentration dependent dielectric, AC conductivity and sensing study of ZnO-polyvinyl alcohol nanocomposite films. *Int. J. Nanotechnol.* **2017**, *14*, 961. [\[CrossRef\]](#)
90. Aziz, S.B. Study of electrical percolation phenomenon from the dielectric and electric modulus analysis. *Bull. Mater. Sci.* **2015**, *38*, 1597–1602. [\[CrossRef\]](#)
91. Mohammed, M.I. Dielectric dispersion and relaxations in (PMMA/PVDF)/ZnO nanocomposites. *Polym. Bull.* **2021**, *79*, 2443–2459. [\[CrossRef\]](#)
92. Aziz, S.B. Role of Dielectric Constant on Ion Transport: Reformulated Arrhenius Equation. *Adv. Mater. Sci. Eng.* **2016**, *2016*, 2527013. [\[CrossRef\]](#)
93. Aziz, S.B.; Abdullah, R.M.; Kadir, M.F.Z.; Ahmed, H.M. Non suitability of silver ion conducting polymer electrolytes based on chitosan mediated by barium titanate (BaTiO<sub>3</sub>) for electrochemical device applications. *Electrochim. Acta* **2019**, *296*, 494–507. [\[CrossRef\]](#)
94. Kobayashi, M.; Mizuno, M.; Aizawa, T.; Hayashi, M.; Mitani, K. Development of Zinc-Oxide Non-Linear Resistors and Their Applications to Gapless Surge Arresters. *IEEE Trans. Power Appar. Syst.* **1978**, *PAS-97*, 1149–1158. [\[CrossRef\]](#)
95. Hemalatha, K.S.; Sriprakash, G.; Prasad, M.V.N.A.; Damle, R.; Rukmani, K. Temperature dependent dielectric and conductivity studies of polyvinyl alcohol-ZnO nanocomposite films by impedance spectroscopy. *J. Appl. Phys.* **2015**, *118*, 154103. [\[CrossRef\]](#)
96. Bin Ahmad, M.; Fatehi, A.; Zakaria, A.; Mahmud, S.; Mohammadi, S.A. Fabrication of an Electrically-Resistive, Varistor-Polymer Composite. *Int. J. Mol. Sci.* **2012**, *13*, 15640–15652. [\[CrossRef\]](#) [\[PubMed\]](#)
97. Abkowitz, M.; Facci, J.S.; Rehm, J. Direct evaluation of contact injection efficiency into small molecule based transport layers: Influence of extrinsic factors. *J. Appl. Phys.* **1998**, *83*, 2670–2676. [\[CrossRef\]](#)



98. Janardhanam, V.; Jyothi, I.; Lee, J.-H.; Kim, J.-Y.; Reddy, V.R.; Choi, C.-J. Electrical Properties and Carrier Transport Mechanism of Au/n-GaN Schottky Contact Modified Using a Copper Pthalocyanine (CuPc) Interlayer. *Mater. Trans.* **2014**, *55*, 758–762. [[CrossRef](#)]
99. Bunakov, A.; Lachinov, A.; Salikhov, R. Current-voltage characteristics of thin poly(biphenyl-4-ylphthalide) films. *Macromol. Symp.* **2004**, *212*, 387–392. [[CrossRef](#)]

**Disclaimer/Publisher’s Note:** The statements, opinions and data contained in all publications are solely those of the individual author(s) and contributor(s) and not of MDPI and/or the editor(s). MDPI and/or the editor(s) disclaim responsibility for any injury to people or property resulting from any ideas, methods, instructions or products referred to in the content.